iScience

CellPress
REVIEWS

Review

Instrumented Microphysiological Systems for Real-Time Measurement and Manipulation of Cellular Electrochemical Processes

Jonathan R. Soucy,[1] Adam J. Bindas,[1] Abigail N. Koppes,[1,2] and Ryan A. Koppes[1,*]

Recent advancements in electronic materials and subsequent surface modifications have facilitated real-time measurements of cellular processes far beyond traditional passive recordings of neurons and muscle cells. Specifically, the functionalization of conductive materials with ligand-binding aptamers has permitted the utilization of traditional electronic materials for bioelectronic sensing. Further, microfabrication techniques have better allowed microfluidic devices to recapitulate the physiological and pathological conditions of complex tissues and organs *in vitro* or microphysiological systems (MPS). The convergence of these models with advances in biological/biomedical microelectromechanical systems (BioMEMS) instrumentation has rapidly bolstered a wide array of bioelectronic platforms for real-time cellular analytics. In this review, we provide an overview of the sensing techniques that are relevant to MPS development and highlight the different organ systems to integrate instrumentation for measurement and manipulation of cellular function. Special attention is given to how instrumented MPS can disrupt the drug development and fundamental mechanistic discovery processes.

INTRODUCTION

Electrical observations of cellular function have been reported as early as the late 18th century with Luigi Galvani demonstrating the link between electricity, the nervous system, and muscle contractions (Bresadola, 1998). However, it was over 200 years later that electrical recordings of muscle cells were collected *in vitro*. In 1972, Thomas et al. were the first to report electrical activity recorded from contracting heart cells isolated from chick embryos on a microelectrode array (MEA) (Thomas et al., 1972). Erwin Neher and Bert Sakmann then devised the first patch clamp system and recorded single ion channels in the membrane of frog skeletal muscle cells (Neher and Sakmann, 1976). Following these seminal demonstrations, great progress in understanding cellular bioelectronics in culture have been made. Yet, a major void remains in our understanding of how individual cellular processes extrapolate into contributions to network, tissue, and organ function *in vivo*. Traditionally, bioelectronic observations *in vitro* have utilized a destructive approach, investigating dissociated cell cultures. Leveraging the developments in microfluidics, tissue engineering, and electronics, a shift to an additive approach to develop three-dimensional (3D), instrumented tissue structures has provided a new path to fully understand bioelectronics from ion channels to organ function (Figure 1).

These engineered cell culture models are frequently termed "organs-on-chips" or "microphysiological systems" (MPS) and are geared toward supplementing drug discovery by predicting *in vivo* efficacy and toxicity (Huh et al., 2012) more accurately compared with static 2D cell cultures. Further, integrated electrical components with real-time outputs offer dynamic measures of cell function through matriculation and environmental or pharmacological interrogation. Whereas MPS technology has yet to be adopted into the pharmaceutical pipeline, microfluidic devices have shown promise with a number of chip designs available from several commercial vendors that provide more uniform nutrient delivery to maintain homeostasis or drive specific chemotactic gradients. A detailed summary of MPS start-ups and their products can be found here (Zhang and Radisic, 2017). However, the majority of commercial products require microscopy to monitor cell function, which limits functional testing. Beyond passive, differential (primary electrode – reference) recordings of muscle and nervous tissues, a number of on-chip sensors have been developed to investigate cell function via bioelectronic properties (Figure 2). Even cells not traditionally considered electrically active can be probed using active, bioelectronic techniques, whereby electric potentials are applied, and current densities are measured (or vice versa) to explore the resistivity and conductance of cell monolayers. These measures can provide real-time insight into cell-cell interactions and

[1]Department of Chemical Engineering, Northeastern University, Boston, MA 02115, USA

[2]Department of Biology, Northeastern University, Boston, MA 02115, USA

*Correspondence: r.koppes@northeastern.edu

https://doi.org/10.1016/j.isci.2019.10.052

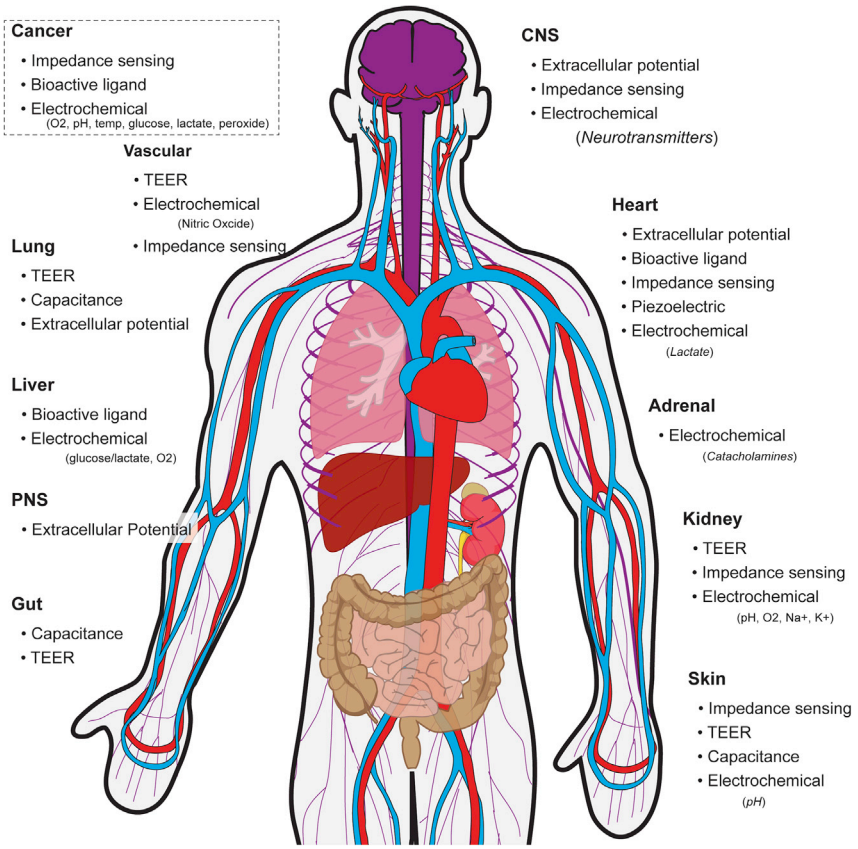

Figure 1. Overview of MPSs across the Body and Modes of Electric-Based Sensing

morphology. This review outlines a number of organ systems that have been recapitulated as MPS as well as the bioelectronic interrogation methods for real-time measures of tissue health, function, and response to exogenous stimuli.

CNS-ON-CHIP

The central nervous system (CNS) is comprised of neurons that communicate via depolarizations of their cell membrane and are responsible for rapidly relaying information throughout the body via the spinal cord and all mental functions in the brain. Eight years after the first recordings of beating cardiomyocytes (CMs) on MEAs, Jerome Pine altered the electrode design to improve signal-to-noise ratio and record extracellular action potentials (APs; Figure 2) of dissociated neuron cultures from superior cervical ganglia of the neonatal rat (Pine, 1980). The adaption of lithographic techniques to manipulate surface chemistry has paved the way for patterning 2D neural structures *in vitro* (Kleinfeld et al., 1988). Patterning of surface coatings with microcontact-printing has been utilized to create simple neural circuits (Jang et al., 2016; Jungblut et al., 2009; Marconi et al., 2012). However, both adhesive and repellant surface coatings, especially finer features (<10 μm), are unstable in culture, often degrading within one week (Wheeler and Brewer, 2010). Additionally, patterning neurons on flat 2D substrates can be influenced by cell migration and motility from tension exerted by neurites, leading to increasing distance between cell bodies and patterned electrodes and thus signal loss (Anava et al., 2009). To overcome these challenges and restrict motility, caging and physical barriers have been implemented to maintain the location of neuron somas in reference to recording electrodes (Zeck and Fromherz, 2001).

In order to further introduce stability, a higher degree of complexity, and 3D culture, microfluidics have been implemented to constrict cell bodies and control axonal growth (Gladkov et al., 2017; Moutaux et al., 2018; Osaki et al., 2018; Pan et al., 2015). Specifically, Kanagasabapathi et al. demonstrated changes in spontaneous extracellular activity of rat cortical neurons constrained along microchannels between two

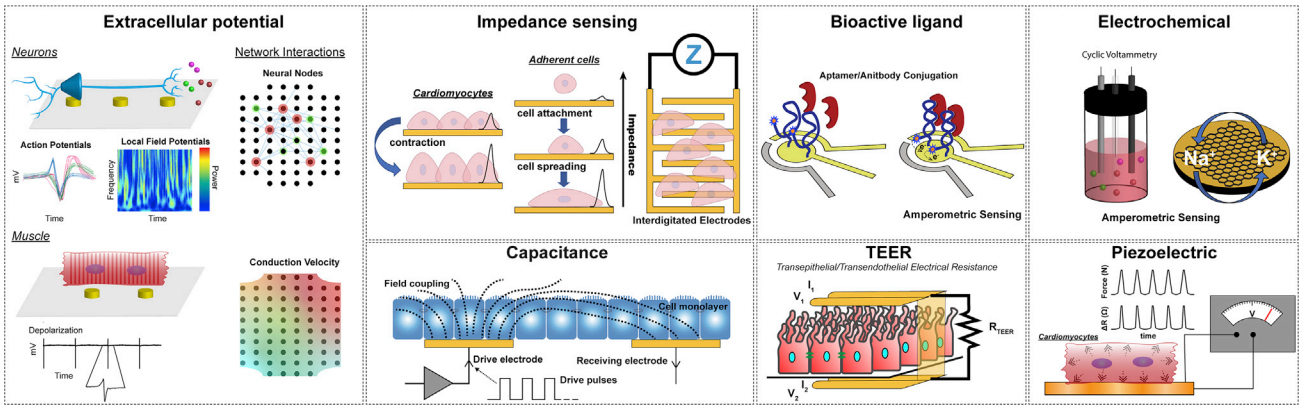

Figure 2. Overview of Types of Passive and Active Electric-Based Sensing Integrated in MPSs

microfluidic compartments (Figure 3A) (Kanagasabapathi et al., 2011). Microchannels were fabricated in polydimethylsiloxane (PDMS) and adhered to commercially available MEAs. Demonstrating an advantage of electrode arrays over patch clamp recordings toward understanding network dynamics, Kanagasabapathi et al. investigated cross-correlations of neural activity spatially (across 60 electrodes, equally spaced; Figure 2) and temporally (binned at 0.1 ms). Further, this team has used this platform for investigating co-cultures of cortical and thalamic neurons (Kanagasabapathi et al., 2012) as well as selective pharmacologic manipulation with tetrodotoxin (Kanagasabapathi et al., 2013). An alternative design with user-friendly, macroscale wells for cell seeding has also been utilized for constraining cortical neuron growth on commercially available MEAs (Figure 3B) (Pan et al., 2015). As computational and cost barriers are overcome, high-density microelectrode arrays are becoming more common with 2D neuron cultures. Lewandowska et al. utilized a >11,000 MEA to study signal propagation along constrained rat cortical neurites in PDMS microchannels (Lewandowska et al., 2015). This platform allowed for the recording of discrete action potentials propagating from the soma to individual neurites or the axonal terminus.

A major hurdle to recording 3D cell cultures is the requirement of electrode-cell intimacy to ensure proper signal-to-noise ratio. Toward 3D hippocampal networks *in vitro*, Rowe et al. demonstrated a tower design of SU-8 pillars to incorporate electrodes and perfusion in an 8 × 8 3D scaffold (Figure 3C) (Rowe et al., 2007). Although recordings for this design were not demonstrated, a similar 3D fluidic and electrode culture platform was implemented for recording spontaneous and evoked activity from cortical neurons for up to 28 days (Figure 3D) (Musick et al., 2009).

Although extracellular, differential recordings are a proven means for recording spontaneous and evoked activity *in vitro*, adding additional functionalities to MPS of the CNS are advantageous for elucidating underlying cellular communication. A thorough review of recording technologies including the use of field effect transistors can be found here (Hong and Lieber, 2019). On chip, electrical impedance measurements between interdigitated electrodes can provide real-time indications of cell adhesion or cytotoxicity (Figures 2 and 3E) (Koester et al., 2010b). Additionally, sensors for respiration (Clark-type oxygen electrodes), acidification (pH-ISFETs), and cell adhesion (interdigitated electrode structures, IDES) have been demonstrated *in vitro* with cortical neurons (Buehler et al., 2011).

PNS-ON-CHIP

MPS of the peripheral nervous system (PNS) have been developed to investigate the underlying mechanisms of regeneration following trauma or the treatment of pain. Focusing on efferents, the PNS is often investigated in the context of motor and cardiac neuroeffector units with muscle contraction as the sole functional output. Pulsatile electrical stimulation (Oiwa et al., 2016), pharmacological stimulation (Smith et al., 2013), and light stimulation of transgenic neurons (Uzel et al., 2016) have been used to evoke neural firing and confirm functional synapsing onto muscle cells. The displacement of passive force transducers (Morimoto et al., 2013; Smith et al., 2013; Uzel et al., 2016), relative fluorescent intensity of Ca^{2+} gradients (Ionescu et al., 2016; Zahavi et al., 2015), and myocyte electrophysiology (Oiwa et al., 2016; Takeuchi et al., 2011) have all been used as quantitative measures of muscle contraction frequency and/or strength in

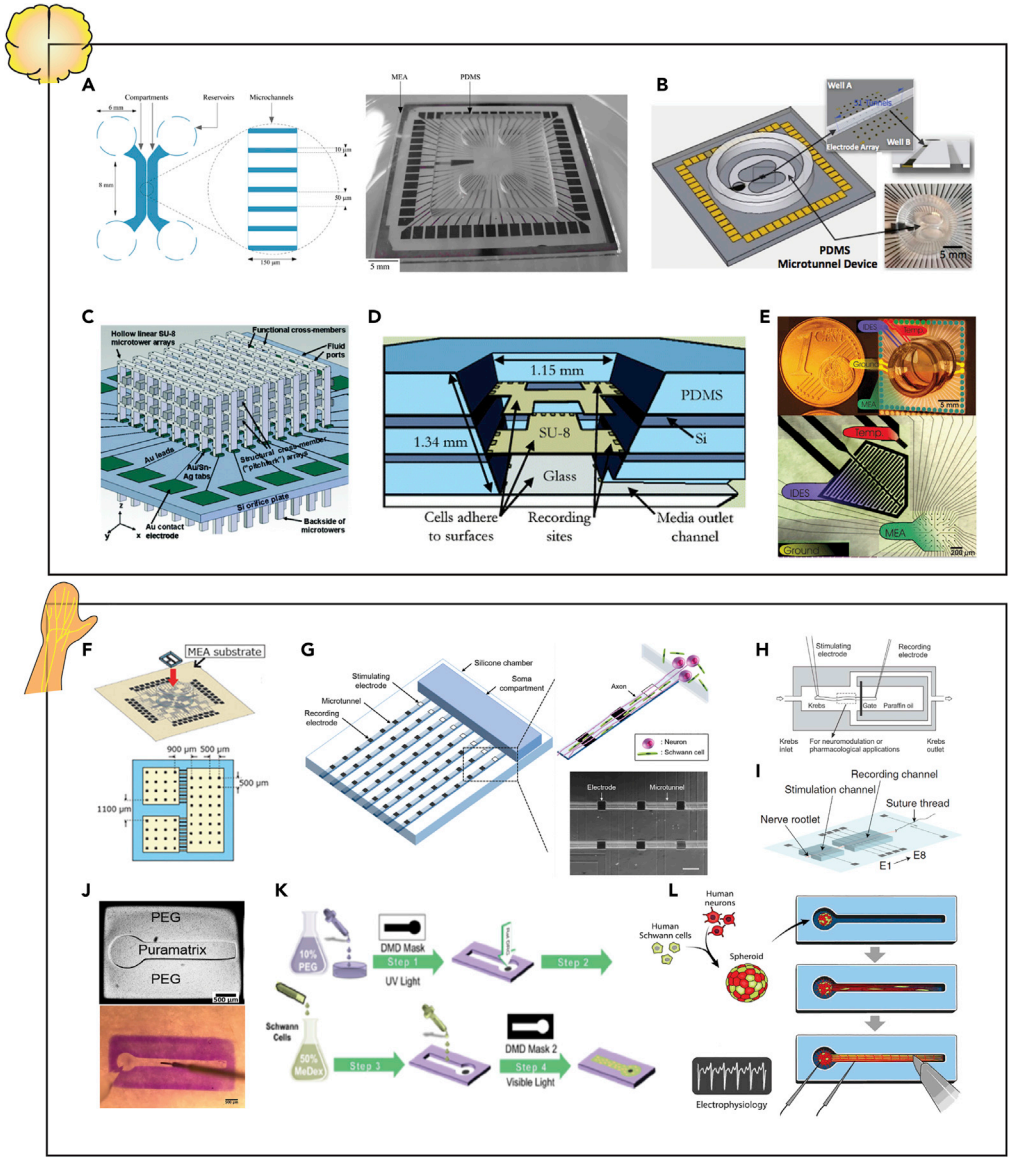

Figure 3. Examples of Instrumented Organ-on-chip Models of the Peripheral and Central Nervous System

(A and B) Extracellular activity and connectivity of compartmentalized cortical neurons via an MEA.

(C and D) Extracellular recordings of neural activity and 3D connectivity via a 3D MEA.

(E) Extracellular recordings and impedance detection to quantify firing frequency and cell adhesion of neuronal cells exposed to sodium valproic acid via an MEA and an interdigitated electrode structure.

(F) Extracellular recordings of spontaneous and stimulated autonomic neuron activity for regulating cardiac beating via an MEA.

(G) CV of myelinated and nonmyelinated sensory neurons via a microchannel-electrode approach.

(H) Single-unit action potentials and CV of intact sciatic nerves exposed to ultrasound stimuli via a multi-wire electrode array.

(I) CAP and CV of intact sciatic nerves via a microchannel-electrode approach.

(J, K, and L) (J) CAP recording in 3D rodent sensory neuron, (K) 3D myelinated rodent sensory neurons, and (L) 3D human stem cell-derived sensory neuron models via stimulating and recording wire electrodes.

Reprinted and adapted with permission from: A (Kanagasabapathi et al., 2011); B (Pan et al., 2015); C (Rowe et al., 2007); D (Musick et al., 2009); E (Koester et al., 2010a); F (Oiwa et al., 2016); G (Sakai et al., 2017); H (Chen et al., 2017); I (Gribi et al., 2018); J (Huval et al., 2015); K (Khoshakhlagh et al., 2018); and L (Sharma et al., 2019). MEA, multielectrode array; CV, conduction velocity; CAP, compound action potential.

response to spontaneous and/or evoke neurogenic control. Further, in addition to contractile properties, myoblasts function as endocrine organs and release cytokines following physical exertion (Pedersen and Febbraio, 2008). Using electrical stimulation Ortega et al. established a skeletal muscle MPS for *in situ* monitoring of secreted interleukin-6 (IL-6) and tumor necrosis factor alpha (TNF-α) via amperometric measurements from immunofunctionalized electrodes (Ortega et al., 2019).

Although measuring the activity of the target muscle to get at the neuromuscular unit can be accomplished by visual and electrical means, disorders such as multiple sclerosis and Guillain–Barré syndrome primarily affect neuron signal transduction and neural-glia interactions (Joy et al., 2001; Winer, 2014). Oiwa et al. established an MPS model of the CNS in which both neural and cardiac electrophysiology was recorded via an integrated MEA (Figure 3F) (Oiwa et al., 2016). Cardiac and neural populations were physically constrained into separate compartments for independent assessment. Similar to the microchannels utilized for studying brain networks, Sakai et al. engineered a microfluidic device with microtunnels positioned atop electrodes to evaluate the contribution of unmyelinating and myelinating Schwann cells (SCs) to regulate axonal conduction (Figure 3G) (Sakai et al., 2017). Using this microtunnel-electrode approach to coculture neurons and SCs, SC coculture was found to increase conduction velocity in a density-dependent manner. However, due to the homologous immature SC populations used *in vitro*, the mature non-myelinating SCs that are important for maintaining axonal conduction velocity *in vivo* were not present within this model (Taveggia et al., 2005).

To overcome the limitations of insufficient cellular heterogenicity, while maintaining the highly controlled environment characteristic of microfluidic-based cell culture techniques, sciatic nerve explants can be integrated *in situ* (Chen et al., 2017; Gribi et al., 2018). Multiple variations of *in vitro* systems for simultaneous recording from multiple axons within a sciatic nerve explant from mice (Figure 3H) (Chen et al., 2017) and from rats (Figure 3I) (Gribi et al., 2018). Chen et al. utilized their platform to demonstrate that ultrasonic stimulation resulted in a temporary increase in nerve conduction velocity following stimuli. Similarly, Gribi et al. demonstrated multiple modes of simulation and electrical recording along the length of the sciatic nerve explant to enable the systematic monitoring and quantification of neural activity from heterogeneous groups of nerve fibers. By investigating both multi-unit and compound action potentials (MUAPs and CAPs), in addition to conduction velocities, the researchers were able to demonstrate the selective heat-induced neuro-inhabitation upon local illumination of an optoelectronic organic semiconductor film. Together, such nerve explant systems represent robust MPS platforms to elucidate the underlying mechanisms of neuromodulation in a dish.

However, despite the potential for using nerve explants within instrumented microfluidic devices for mechanistic studies and preclinical drug screening, there is a limited supply of healthy human donor nerves. Further, removal and maintenance of an intact sciatic nerve is technically challenging and requires sufficient time and resources, thereby limiting experimental throughput. Using primary rodent cell sources, Huval et al. microengineered a biomimetic sensory neural fiber tract model capable of electrophysiological and histopathological assessment (Figure 3J) (Huval et al., 2015). Rat embryonic dorsal root ganglia (DRGs) were encapsulated in a PuraMatrix hydrogel and spatially confined in a growth resistance polyethylene glycol (PEG) hydrogel with a geometry resembling nerve fiber tracts. The neural response to known Na+ channel and glutamate blockers were then observed via recording electrodes at the nerve bulb and along neurite outgrowth to measure CAP. Beneficially, the dual hydrogel system allows the culture to be fixed and sectioned for transmission electron microscopy (TEM) of neural culture cross-sections to investigate myelination. To further explore myelination *in vitro*, the platform was modified to incorporate exogenous SCs (Figure 3K) (Khoshakhlagh et al., 2018). Using a growth-restrictive PEG hydrogel to confine nerve tracts, rat neonatal SCs were encapsulated along with rat embryonic DRGs in a glycidyl methacrylate-dextran hydrogel. Using TEM, the ratio of myelin to βIII-tubulin was significantly greater with longer exposure to ascorbic acid and addition of endogenous cells, indicating the formation of SCs from the proliferative to the myelinating phenotype. However, due to the opacity of the dextran-based hydrogel, electrode positioning was a major challenge in chips containing exogenous SCs. Nevertheless, the addition of ascorbic acid alone to DRGs containing endogenous SCs increased the signal amplitude and nerve conduction velocity.

Despite these current advances in *in vitro* models of the PNS, there are underlying biological differences between rodent and human cells that need to be studied for improving the predictivity of preclinical

drug screening (van der Worp et al., 2010). Sharma et al. developed a human sensory neural fiber tract model using the same growth-restrictive approach previously described (Figure 3L) (Sharma et al., 2019). Spheroids of human motor neurons and human SCs were developed and cultured in a Matrigel hydrogel that was spatially confined by a polyethylene glycol dimethacrylate 1000 hydrogel. Ascorbic acid was shown to increase myelination within SC/neuron coculture, but contradictory to results described *in vivo*, nerve conduction velocity was found to be slower than unmyelinated neurons. Although there are several theories to examine this surprising finding, continued effort is required to fully mimic the PNS *in vitro*.

HEART-ON-CHIP

CMs maintain their phenotype in culture, spontaneously contracting with large ion fluxes across their membranes. For this reason, CM biophysics have been robustly characterized and used as test beds for engineering developments in electrophysiology (e.g., first demonstration of MEA recording). Further, cardiovascular disease is the leading cause of death worldwide, driving a breadth of ongoing research (Bank et al., 2015). To improve the *in vitro* to *in vivo* translatability of cardiac models, it is critical to reconstitute the vasculature-like perfusion, cell-tissue interactions, and electroactive function of the heart (Bhatia and Ingber, 2014; Ingber, 2016). Consequently, advancements in microfabrication and the advent of human-induced pluripotent stem cell (iPSC)-derived CMs have pushed the field to engineer instrumented heart-on-chip models that better mimic human physiology and quantify real-time outputs of cardiac function (Kitsara et al., 2019).

Extracellular measurements of cardiac electrophysiology *in vitro* can be directly related to the human heart's electrical cycle (Braam et al., 2010; Caspi et al., 2009). MEAs remain as the gold standard for assessment of CM electrophysiology *in vitro* (Spira and Hai, 2013). Using an MEA, firing frequency or beat rate, field potential amplitude and its duration, as well as population measures, including conduction velocity (Figure 2), can be recorded and monitored in real-time (Denning et al., 2016). Kujala et al. micromolded gelatin atop a commercially available MEA to pattern human iPSC-derived CMs to improve biocompatibility via a more mechano-physiological substrate (Figure 4A) (Kujala et al., 2016). Despite this hydrogel layer (~86 μm), signal-to-noise ratios remained sufficient to carry out dosage assays with isoproterenol (Kujala et al., 2016). In this work, to mimic vasculature-like perfusion, chemically and biologically inert polyether-ether-ketone (PEEK) microfluidics were employed.

Although previous models clearly demonstrated the importance of both vasculature-like flow and integrating MEAs on-chip for assessing the efficacy or toxicity of pharmacological compounds, accurate pharmacodynamic *in vitro* modeling requires vasculature-like perfusion through endothelium-lined microchannels (Ingber, 2016). To that end, Maoz et al. engineered a vascularized, bilayer heart-on-chip model with endothelial cell monolayers cultured on a transmembrane above human iPSC-derived CMs (Figure 4B) (Maoz et al., 2017). The custom dual channel design integrated both an MEA substrate and platinum black-coated gold electrodes for transepithelial electrical resistance (TEER) measurements (Figure 2) to simultaneously evaluate both cardiac electrophysiology and endothelial barrier function. TEER is a direct measure of bioimpedance, typically utilized on a tightly formed monolayer resistant to the passive flow of ions in cell media. These measurements are critical for understanding kinetics and dynamics of pharmaceuticals and help to quantify the ionic conductance of the paracellular junctions through a cell monolayer and reflect the integrity of epithelial barrier (Hickman, 2016). Maoz et al. validated the efficacy and resolution of this multifunctional platform by simultaneously disrupting the endothelial barrier integrity with an inflammatory cytokine (TNFα) and administering isoproterenol to increase beat rate and field potential duration, as confirmed with TEER and an MEA, respectively (Maoz et al., 2017).

The electrodes of standard, 60-channel, MEAs can be individually addressed with a function generator or potentiostat, allowing for electrical stimulation (Cheng et al., 2010; Ma et al., 2011), electrochemical detection of cardiac biomarkers (Cheng et al., 2010; Shin et al., 2016; Zhang et al., 2017), and application of direct and alternating electric fields on-chip (Tandon et al., 2010; Yang and Zhang, 2007). Exogenous pacing of CMs is a critical assessment of the contractile and intracellular connectivity (Tandon et al., 2009), and therefore needs to be considered when developing cardiac MPS models (Cimetta et al., 2013). Ma et al. established an MEA-based biochip for stimulating cells found within the myocardium to investigate signal propagation (Ma et al., 2011).

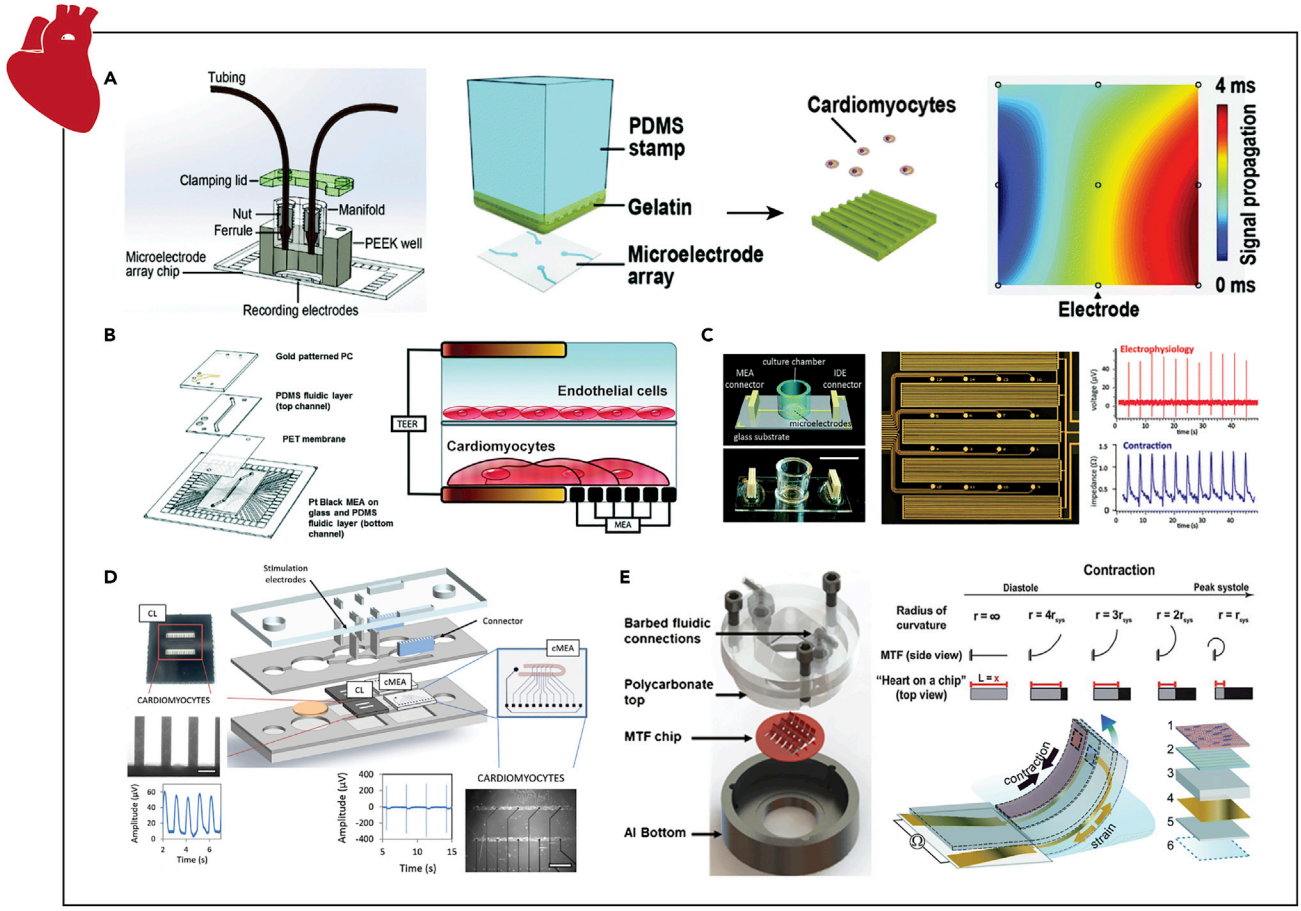

Figure 4. Examples of Instrumented Organ-on-chip Models of the Heart

(A) Extracellular recordings of micropatterned stem-cell-derived CMs to study cardiac beating, field potentials, and conduction velocity via an MEA under vascular-like perfusion.

(B) Extracellular field potential duration and beat rate measurements from a CM/endothelial cell bilayer coculture model to assess the pharmacodynamics of altered vascular permeability via an MEA.

(C) Concurrent assessment of cardiac electrophysiology, beat rate, contractility, and viability via an MEA and IDEs with interpenetrating geometries for measuring field potentials and impedance, respectively.

(D) Parallel quantification of cardiac contraction force and electrophysiology of patterned stem-cell-derived CMs via independent cantilever system and MEA, respectively.

(E) Real-time cardiac tissue force quantification via the change in resistance caused by the deformation of piezoelectric MTF chips.

Reprinted and adapted with permission from: A (Kujala et al., 2016); B (Maoz et al., 2017); C (Qian et al., 2017); D (Oleaga et al., 2019); and E (Agarwal et al., 2013; Grosberg et al., 2011; Lind et al., 2017). CMs, cardiomyocytes; MEA, multielectrode array; IDEs, interdigitated electrodes; MTF, muscle thin films.

To garner a deeper understanding of ischemic heart damage, Cheng et al. fabricated a custom five electrode MEA, containing two platinum pacing (20 μm wide and 200 μm apart), one platinum counter (30 μm wide), and one Ag/AgCl reference (20 μm wide) electrode, in addition to a lactate electrochemical working electrode (50 μm wide), to manipulate and monitor single adult rabbit CMs (Cheng et al., 2010). The reference electrode was positioned away from the CMs, as AG can be toxic to cells. To establish the lactate biosensor as a metabolic indicator of cardiac ischemia, lactate oxidase was trapped onto the electrode surface with a poly(o-phenylenediamine) film so that in the presence of lactate the electroactive species would easily diffuse to the electrochemical interface. As an alternative to a polymer entrapped enzyme, Shin et al. and Zhang et al. both report on the development and use of an aptamer- and antibody-based (Figure 2) creatine kinase (CK)-MB biosensor within an MPS to investigate human cardiotoxicity (ESC and iPSC derived) to pharmacological compounds, respectively (Shin et al., 2016; Zhang et al., 2017). Yang et al. demonstrated that by applying an electric field within a microfluidic device, adult rat CMs were aligned along the field's direction and formed a biomimetic tissue-like structure (Yang and Zhang, 2007). Similarly, Tandon et al. showed that with electrical simulation, neonatal rat CMs exhibited enhanced alignment

and elongation within a custom PDMS-based bioreactor mounted to an optically clear indium tin oxide MEA (Tandon et al., 2010).

Larger interdigitated electrodes (IDEs) have been used to assess CM mechanical function via high-resolution ECIS, measuring changes in bioimpedance across confluent, contracting cell monolayers. Beat rate and cell viability can also be noninvasively monitored with this technique (Nguemo et al., 2012; Zhang et al., 2016), both of which are powerful predictive tools for preclinical pharmaceutical efficacy and safety (Abassi et al., 2012). Toward developing heart-on-chip technologies to assess the cardiotoxicity during the drug discovery process, Zhang et al. fabricated a microfluidic device to culture neonatal rat CMs on IDEs (Zhang et al., 2016). Proof-of-concept studies confirmed that the verapamil decreased both beat rate and contractility (lower signal amplitude) while not affecting cell viability and that doxorubicin decreased beat rate, contractility, and viability. Qian et al. integrated an MEA and an IDE with interpenetrating geometries to assess cardiac electrophysiology, in addition to quantifying beat rate, contractility, and viability from impedance readouts (Figure 4C) (Qian et al., 2017). Further, due to the overlapping MEA/IDE geometries, this platform was used to electrically stimulate human iPSC-derived CMs and generate field potential maps under physiological conditions and pharmacological stimuli in real-time. Using this cardiac model with interdigitated MEAs and IDEs, the addition of norephedrine, a clinical drug used to treat low blood pressure and heart failure, demonstrated several physiological effects on CM outputs only observable with simultaneous readouts from combinational electrode arrays.

Although impedance offers an indirect measure of cardiac contractile force, the signal measured may be influenced by protein adsorption or electrode degradation over time and/or when introducing drugs as well as relying on a confluent monolayer (Qian et al., 2017). Specifically, ECIS is influenced by the osmotic concentration of the medium, erroneous bioimpedance signals from noncontractile cells and extracellular proteins/molecules, and the total adhesion to the IDE, all of which are highly variable (Heileman et al., 2013). Therefore, as an alternative to impedance spectroscopy, researchers have directly measured contractile force with microfabricated pillars/cantilevers (Boudou et al., 2012; Zhao and Zhang, 2006), video microscopy of flexible film substrates (Feinberg et al., 2007), calcium imaging (Huebsch et al., 2015), and visual tracking of either magnetic or fluorescent beads in materials of known moduli (Aung et al., 2015; Yin et al., 2005). In combination with an MEA, Oleaga et al. developed an MPS that incorporates an independent cantilever system for monitoring mechanical and electrophysiological function in the heart (Figure 4D) (Oleaga et al., 2018, 2019). This platform was used to both evaluate the long-term cardiotoxicity in a multi-organ system (Oleaga et al., 2019) and better predict the pharmacokinetics/pharmacodynamics (PK/PD) of preclinical drug molecules (Oleaga et al., 2018). The combination of electrical readouts and contractile force has a high predictive value for parameters associated with drug-induced cardiotoxicity: spontaneous beating rate, conduction velocity, QT interval, minimal inter-spike interval, peak contractile force, speed of contraction, and rate of relaxation (Stancescu et al., 2015).

Despite the need for laborious optical analysis and dedicated microscopy setups, often visual deformation of materials to measure contraction force is still used within microfluidic devices for real-time readouts of cardiac contractility (Aung et al., 2015; Lind et al., 2016). For example, Agarwal et al. incorporated muscle thin films (MTFs) into a microdevice with fluidic fittings and a heated base for maintaining vasculature-like flow and physiological temperatures, respectively (Figure 4E) (Agarwal et al., 2013). In addition, to optically record deformation of the MTFs, which is associated with the contractility of the cardiac tissue, the devices were fabricated with a transparent top. Lastly, imbedded electrodes enabled the electrical field stimulation of the cardiac tissue constructs. However, to remove the need for microscopy-based force measurements, piezoresistive, high-conductance, and flexible biocompatible inks were printed onto MTFs (Lind et al., 2016). These embedded sensors provided non-invasive, real-time, continuous electrical readouts of cardiac contractile stresses within an MPS. Although this device allows for a function output across a battery of testing parameters, indications on cellular electrophysiology and population signal propagation are limited.

ADRENAL-ON-CHIP

The adrenal glands function as the effector organ, preparing the body to respond to stress (Olson et al., 2011). Part of a sympathetic division, adrenal chromaffin cells located in the medulla release glucocorticoids, epinephrine (EP), and norepinephrine (NEP) into the periphery to initiate the "flight-or-fight" response. The fast release of these glucocorticoids relies on membrane depolarizations similar to the

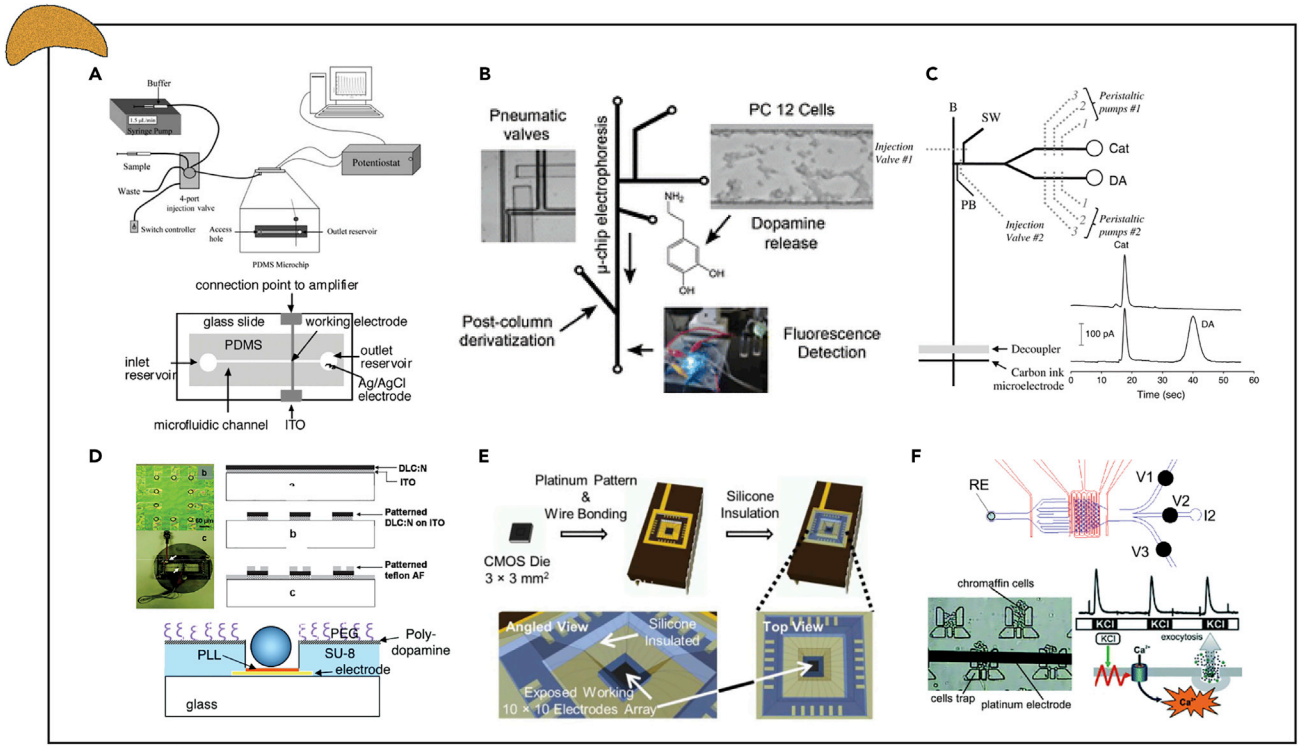

Figure 5. Examples of Instrumented Organ-on-chip Models of the Adrenal Gland

(A) Amperometric detection of catecholamines released from immobilized PC12 cells after calcium/potassium stimulation via platinum/indium tin oxide electrodes.

(B) Fluorescent detection of dopamine release from immobilized PC12 cells via electrophoretic-based separation of catecholamines.

(C) Simultaneous electrochemical detection of dopamine and norepinephrine from immobilized PC12 cells via microchip electrophoresis and carbon ink microelectrodes.

(D) Electrochemical detection of single-cell catecholamine exocytosis from cytophobically/fluidically trapped bovine chromaffin cells via a multielectrode array.

(E) Electrochemical detection of catecholamines from multiple individual bovine chromaffin cells via a 10 × 10 potentiostat electrode array.

(F) Spatiotemporal amperometric spike detection from bovine chromaffin cell clusters in repose to physiologically relevant secretagogues to assess the kinetics of adrenal catecholamine exocytosis via interdigitated electrodes.

Reprinted and adapted with permission from: A (Li et al., 2005; Sun and Gillis, 2006); B (Li and Martin, 2008); C (Bowen and Martin, 2010); D (Barizuddin et al., 2010; Liu et al., 2011); E (Kim et al., 2013); and F (Ges et al., 2013).

APs of neurons and muscle (de Diego, 2010). Chromaffin cells exhibit a resting potential of ~−50 mV and APs (~65 mV) in a frequency range between 0.2 and 3 Hz, a similar range to the resting (0.2 Hz) and stressed discharge from the sympathetic-splanchnic nerve (de Diego et al., 2008). From measuring glucocorticoid production to monitoring exocytosis events, the adrenal medulla possesses a number of attributes that make it amenable to bioelectronic interrogation.

To effectively distribute these catecholamines systemically, the adrenal glands require a large blood supply and extensive vascularization (Megha and Leslie, 2019). Once in circulation, EP and NEP bind to the adrenergic receptors expressed throughout the body to elicit a physiological response (Byku and Mann, 2016; Ripplinger et al., 2016). Microfluidic-based cell culture techniques are well suited to recapitulate the highly vascularized adrenal microenvironment and mimic tissue perfusion. Moreover, quantal catecholamine release can be readily measured by integrating electrochemical sensors on-chip to detect oxidization (Ges et al., 2012). Li et al. designed a microchannel device for amperometric monitoring of catecholamine transient exocytosis under a continuous flow rate (Figure 5A) (Li et al., 2005). In this study, adrenal chromaffin cells, from rat pheochromocytoma (PC12), were immobilized within a microchannel and repeatedly stimulated with calcium solution to release catecholamines. Similarly, Sun et al. fabricated an instrumented microchannel-based device to investigate quantal catecholamine release from bovine adrenal chromaffin cells in response to perfusion with a potassium solution (Sun and Gillis, 2006). Lastly, as an alternative to

ionic or pharmacological secretagogues, which are often time delayed due to flow and diffusion limitations, a 5 s voltage pulse elicited quantal exocytosis from chromaffin cells within microchannel-based devices (Dittami and Rabbitt, 2009).

NEP and EP concentrations can be differentiated from one another by detecting the second oxidation peak in EP that is not present in NEP, using background-subtracted cyclic voltammetry (Figure 2) (Pihel et al., 1994). Catecholamine concentrations may then be calculated by defining current- and voltage-based calibration parameters from a standard solutions (Wolf et al., 2016). However, in the case of complex tissue systems, it is not possible to distinguish between dopamine and NEP with electrochemical detection of oxidation (Michael and Wightman, 1999). Using a variant of their previously designed chip to immobilize PC12 cells in a microchannel (Li et al., 2005), Li et al. reports that by integrating an electrophoresis channel, dopamine can be separated by mass and charge from NEP and then fluorescently detected (Figure 5B) (Li and Martin, 2008). Further, incorporating peristaltic pumps into a modified microfluidic design enables continuously electrochemical detection of both dopamine and NEP from immobilized PC12 cells (Figure 5C) (Bowen and Martin, 2010).

Despite providing measures of adrenal neurosecretions in the culture medium, systems with only one electrochemical catecholamine detector lack temporal resolution information and often require large cell populations (Ges et al., 2013). Consequently, the Gillis group designed custom MEAs for single cell capture to improve the temporal resolution of quantal exocytosis events (Figure 5D) (Barizuddin et al., 2010; Gao et al., 2013; Liu et al., 2011). In this work, cell-sized microwells were established on MEAs by regulating cell attachment with either Teflon (Barizuddin et al., 2010) or polyethylene glycol (Liu et al., 2011) or by manipulating fluidic flow within a layered device (Gao et al., 2013). Cell trapping efficiency and stability of each device were assessed, and single-cell catecholamine exocytosis was investigated with a potassium secretagogue. Although these techniques provide exquisite sensitivity and temporal resolution of quantal exocytosis, single-cell analysis fails to mimic the packing density of chromaffin cells in the adrenal gland.

In vivo, chromaffin cells rely on autocrine/paracrine communication to regulate catecholamine secretion in response to various stressors (Currie, 2010). Kim et al. established a 100-electrode CMOS-based electrode array for the electrochemical detection of catecholamines from multiple individual chromaffin cells (Figure 5E) (Kim et al., 2013). Single-cell amperometric spikes were detected and corelated to provide spatiotemporal dynamics. To incorporate both autocrine/paracrine communication and vascular-like flow, Ges et al. established a microfluidic culture model with U-shaped cell traps and large, thin film platinum electrochemical electrodes to enable continuous fluidic flow and higher resolution of catecholamine secretion (Figure 5F) (Ges et al., 2013). Using this system, the need for a recovery period between simulations confirmed the impact of repetitive stimulation on kinetic parameters. Lastly, to assess the potential of this system as a sympathoadrenal module to investigate endocrine control of cardiac myocytes and other relevant targets downstream within the device, stimulation of catecholamine exocytosis was investigated using a variety of physiologically relevant secretagogues.

VASCULAR-ON-CHIP

Due to the critical role blood perfusion has in maintaining tissue functions, several MPS that recapitulate vascular physiology have been developed (Lee et al., 2018). A prime example, the blood brain barrier (BBB) is complex multicellular multilayer endothelium that protects and maintains the CNS. The BBB is selectively permeable to essential compounds such as selected sugar, amino acids, electrolytes, hormones, and water, while excluding most other exogenous compounds present in the blood such as select pharmaceuticals and pathogens (Hawkins and Davis, 2005). Toward understanding the underlying mechanisms and developing compounds to cross this barrier, biomimetic BBB models have been developed to investigate the pharmacodynamics of various drug compounds. Conventionally, BBB permeability has been assessed using Transwell inserts, but by establishing flow-based systems with more realistic dimensions and geometries, barrier integrity can be improved to better mimic physiology (van der Helm et al., 2016).

Douville et al. reports on the first microfluidic device with integrated TEER electrodes for real-time assessment of BBB permeability *in vitro* (Figure 6A) (Douville et al., 2010). Mouse-brain-derived endothelial cells (bEnd.3) were cultured on the membrane of a dual-layer PDMS microfluidic chip and were confirmed to establish tight junctions via an increase in TEER results. To further validate use the resolution of this system,

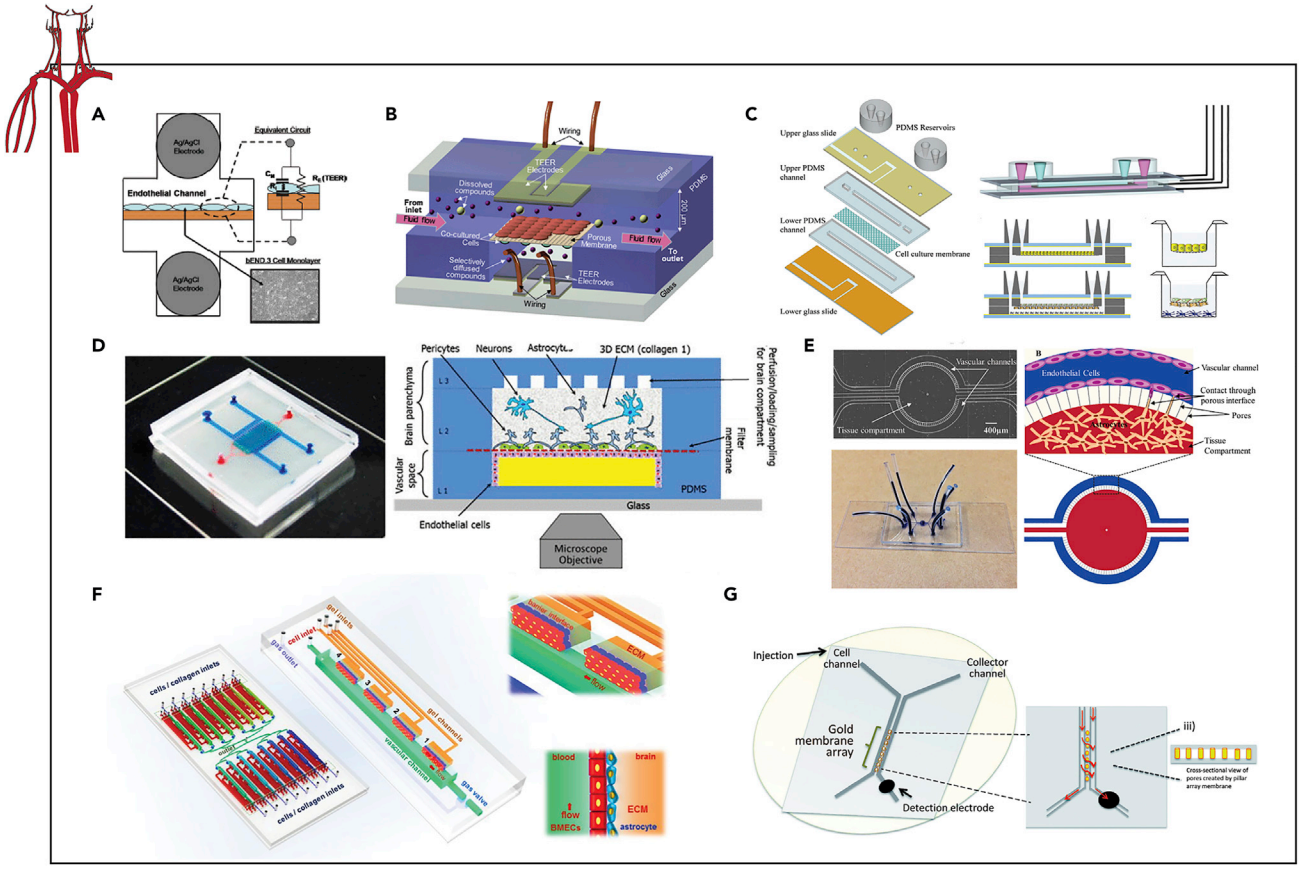

Figure 6. Examples of Instrumented Organ-on-chip Models of the Vasculature System

(A) Permeability study of a mouse-brain-derived endothelial cell (bEnd.3) monolayer cultured on the membrane of a bilayer chip via TEER electrodes.

(B) Barrier integrity assessment of bEnd3 cell monolayer cocultured with a murine astrocytic cell line (C8D1A) in a multilayer chip under flow via TEER.

(C) Human brain endothelial cell line (hCMEC/D3) tight junction integrity investigated within a bilayer chip with vasculature-like flow via TEER electrodes.

(D) BBB integrity assessed within a perfusable trilayer chip, containing brain endothelial cells, astrocytes, and pericytes, in response to physiological stresses via TEER electrodes.

(E and F) (E) BBB permeability quantified in using a 2D and (F) 3D side-by-side orientated vascular channel and the brain compartment microfluidic device via TEER electrodes.

(G) Electrochemical assessment of red blood cell nitric oxide production via an integrated amperometric detector.

Reprinted and adapted with permission from: A (Douville et al., 2010); B (Booth and Kim, 2012); C (Walter et al., 2016); D (Brown et al., 2015); E (Deosarkar et al., 2015); F (Xu et al., 2016); and G (Selimovic et al., 2014). TEER, transepithelial electrical resistance; BBB, blood brain barrier; IDEs, interdigitated electrodes.

TEER values were reduced with the addition of TritonX-100. Endothelial cells are greatly affected by the forces exerted by fluid flow, and Booth et al. established the first instrumented, flow-based, co-culture BBB system (Figure 6B) (Booth and Kim, 2012). A co-culture of bEnd3 cells with a murine astrocytic cell line (C8D1A) under flow exhibited TEER values exceeding 250 $\Omega.cm^2$, compared with 25 $\Omega.cm^2$ in Transwell co-cultures. Shear stress as well as coculturing astrocytes and endothelial cells resulted in higher TEER values. Using the same chip design, Booth et al. further confirmed the predicative potential of their dynamic microfluidic BBB model for investigating the permeability of neuroactive drug molecules (Booth and Kim, 2014). In this study, inclusion criteria for TEER values was established for seeded MPS to decrease sample variability prior to pharmacological interrogation. Jeong et al. iterates on this proven bilayer chip design to expand the throughput of each device for preclinical and mechanistic investigations (Jeong et al., 2018). In this work, a 4 × 4 array of intersecting microchannels forming 16 independent testing areas between the electrodes of two MEAs is used to measure TEER. Leveraging this increased capacity, this platform was used to evaluate a broad experimental range of the extracellular matrix compositions and flow rates or shear stress.

To improve the relevance to human physiology, Griep et al. established a dual-layer PDMS chip with immortalized human brain endothelial cell line hCMEC/D3 cultured on a membrane (Griep et al., 2013). As reported previously in rodent system, high shear stress positively influenced barrier tightness and increased TEER values of a hCMEC/D3 cell monolayer (Griep et al., 2013), whereas low shear stress led to no changes in TEER (Figure 6C) (Walter et al., 2016). As a proof-of-concept, stimulation with tumor necrosis factor alpha (TNF-α) adversely affected barrier integrity and decreased TEER values (Griep et al., 2013). Similarly, Brown et al. developed a human BBB model to assess barrier integrity in response to a cytokine cocktail (Figure 6D) (Brown et al., 2015, 2016). However, to better recapitulate the neurovascular unit, Brown et al. established cell-to-cell communication between endothelial cells, astrocytes, and pericytes. Using an instrumented trilayer PDMS chip, primary human brain–derived microvascular endothelial cells (hBMVEC), primary pericytes and astrocytes, and human iPSC-derived neurons were cultured together to study BBB permeability in response to stress. In this study, cold shock, reduced nutrient perfusion, and neuroinflammation all resulted in a decrease in TEER values, thereby demonstrating the susceptibility of BBB.

Although these multi-layer PDMS chip designs have been invaluable for studying pharmacodynamics and biological mechanisms, their stacked design limits visual monitoring of cellular process. To overcome this limitation, Deosarkar et al. developed a side-by-side orientation of the vascular channel and the brain compartment (Figure 6E) (Deosarkar et al., 2015). However, due to the differences in surface area and pore density, TEER values cannot be directly compared with values obtained from Transwells or multilayered devices. Nevertheless, TEER increased for primary neonatal rat brain capillary endothelial cells when cocultured with primary rat astrocytes, demonstrating comparable results using a side-by-side model. Using a similarly designed system, Xu et al. demonstrated that the coculture of primary adult rat brain microvascular endothelial cells (BMECs) and primary neonatal rat cerebral astrocytes under flow had the highest TEER values compared with iterations of static and monoculture (Figure 6F) (Xu et al., 2016). Using the dynamic coculture model, researchers were then able to study metastases and lipophilic, hydrophilic, or prodrug transport across the BBB.

Besides a limited capacity to monitor cellular processes in multi-layer PDMS chip, the use of PDMS can adversely affect pharmacological studies by absorbing charged small drug molecules and proteins (Toepke and Beebe, 2006; van Meer et al., 2017). Consequently, Falanga et al. developed an poly(methyl methacrylate) (PMMA) microfluidic device to investigate the effectiveness of a membranotropic peptide to shuttle cargo across the BBB layer under flow conditions that mimic circulation (Falanga et al., 2017). PMMA was milled into microchannels with holes to integrate the Pt electrodes for TEER measurement. TEER was used to assess bEnd.3 cell monolayer integrity before and after dosing to confirm that barrier function was not disrupted as a result of the nanocarrier. As an alternative to micromilling, Wang et al. 3D printed an acrylic-based microfluidic device with integrated electrodes to support and assess the coculture of human iPSC-derived BMECs and rat primary astrocytes (Wang et al., 2017). The printed device was coated with a thin layer of parylene-C to ensure chemical resistance and biocompatibility, and 0.8 mm diameter Ag/AgCl pellet electrodes were embedded in the both the bottom and lid layers. Using this model, Wang et al. demonstrated sustained TEER >2000 Ω cm2 for up to 10 days.

In addition to models of the BBB, TEER has been used for real-time monitoring barrier integrity within peripheral, microtube-inspired blood vessel models (Vogel et al., 2011). Vogel et al. established an instrumented MPS to support bovine pulmonary artery endothelial cells for studying interactions with a flowing stream of red blood cells (RBCs). In this work, TEER was used to assess both confluency and barrier integrity prior to investigating the response to RBC adenosine triphosphate (ATP) secretion. Critically, by monitoring TEER values, decoupling of cell barrier integrity and cell proliferation on endothelial nitric oxide (NO) production was achieved. To study NO production electrochemically, Selimovic et al. established an on-chip blood vessel model with an integrated amperometric detector (Figure 6G) (Selimovic et al., 2014). Using this planar, pillar array device, researchers demonstrated that NO release from hypoxic RBCs was detected on glassy carbon/Pt-black/0.05% Nafion electrodes in a cell-free region of the microchip. Such a design prevents the electrode from being coated or passivated by cell adhesion and may be combined with TEER systems so that NO production can be monitored without the need for fluorescence detection.

Although paracrine signaling plays an essential role in the vascular system, cell-cell interactions are just as important to study to recapitulate vascular physiology. Recently, Rothbauer et al. incorporated an impedance spectroscopy-based system to assess cell-cell interactions between smooth muscle cells and endothelial cells in response to an allergen (Rothbauer et al., 2019). Using a dual compartment microfluidic device, an endothelial cell monolayer was cultured atop a layer of smooth muscle cells to establish a biomimetic vascular coculture downstream an immune cell culture. Nitride-coated silicon IDEs were used to monitor impedance (highest resolution observed: 80–100 kHz), both basophil degranulation and vascular coculture interactions. Both the dosing of immune cells with an antigen and the direct administration of histamine to the vascular coculture resulted in cell relaxation and reduction in impedance.

GUT-ON-CHIP

The gut as a system functions to absorb nutrients while acting as a barrier to protect the body from pathogens and is a common and desirable site for drug delivery (Koziolek et al., 2016). As such, significant work has been carried out to understand absorption of orally dosed pharmaceutical interventions through the epithelial lining of the gut into the body (Bein et al., 2018; Kim et al., 2012, 2016b). More recently, the role of the gut's microbiome in tandem with the host's own local cells (i.e. epithelial, immunological, neuronal, muscular, etc.) has been implicated in playing a role in a growing number of health conditions ranging from obesity and heart disease to depression and Alzheimer disease (Butler et al., 2019; Shah et al., 2016). Both drug absorption and basic biological research have found limitations from complete reliance on *in vivo* models to study these phenomena, which has motivated development of more relevant, 3D *in vitro* models, including various geometries of microfluidic chips comprised of primary and immortalized epithelial cells from human biopsies and animal samples (Bein et al., 2018; Kim et al., 2016b; Shah et al., 2016).

Similar to vascular tissue, impedance spectroscopy has been the most extensively implemented biosensor in gut microfluidic chips. Kim et al. first developed a gut microfluidic device whereby TEER was measured every 1–3 days by inserting Ag/AgCl electrode wires (Figure 7A) (Kim et al., 2012). Barrier function was measured in response to the addition of an intestinal microbe (*Lactobacillus rhamnosus* GG) and application of flow. This work was continued whereby a more robust combination of factors (microbe, lipopolysaccharide, *E. coli*) were evaluated for their influence on monolayer integrity (Kim et al., 2016b). Finally, the method of fabrication and operation was detailed in a JoVE article (Kim et al., 2016a). Shah et al. developed a modular, spiraled co-laminar microchanneled device and dubbed the HuMiX to evaluate TEER by directly inserting commercially available chopstick electrodes (STX2; Millipore) commonly utilized for Transwell cultures (Figure 7B) (Shah et al., 2016). Further, the incorporation of 5-mm oxygen sensors (pst3 optodes; PreSens) permitted the application of an oxygen gradient found in the body, which enabled the system to approach anaerobic conditions (<1% O2) and co-colonize the bacteria Lactobacillus rhamnosus GG and Bacteroides caccae (an obligate anaerobe). Throughout culturing, TEER was utilized to evaluate barrier function in response to the presence of bacteria.

Toward integrating TEER electrodes into the MPS platform, Henry et al. developed a PDMS chip that included four gold electrodes patterned on polycarbonate (2 sets of 1 mm wide; 1 mm separation) (Figure 7C) (Henry et al., 2017). Impedance spectra were collected for a broad range of frequencies (10 Hz–100 kHz) to better define cell function and the influence of the resistance of the ionic solution measured at frequencies >10 kHz. From this data, TEER and cell capacitance were calculated from a modified cell equivalent circuit. Cell capacitance directly correlates to the surface area of the cell monolayer and can be utilized to normalize TEER data for influences of variable geometries. Digging deeper into the utilization of impedance spectroscopy, van der Helm et al. developed a method of combining impedance measurements to measure TEER in a fashion that could be compared between systems, which they confirmed by developing integrated 6-electrodes into a layered gut chip to mitigate the influence of double-layer capacitance at the electrode-electrolyte interface (Merrill et al., 2005) as well as resistances within the contacts or lead wires (Figure 7D) (van der Helm et al., 2019). Additionally, the group established electrical simulations of the gut chip as a 2D electrical network in MATLAB to better inform electrode placement as well as indications of barrier function and degree of maturation (i.e., villi formation). Traditional TEER measurements (10 μA at 12.5 Hz) are susceptible to heterogeneity in monolayers, membrane geometry, and electrode placement. Although standard values have been established for Transwell cultures, substantial work remains to equate data across custom MPS.

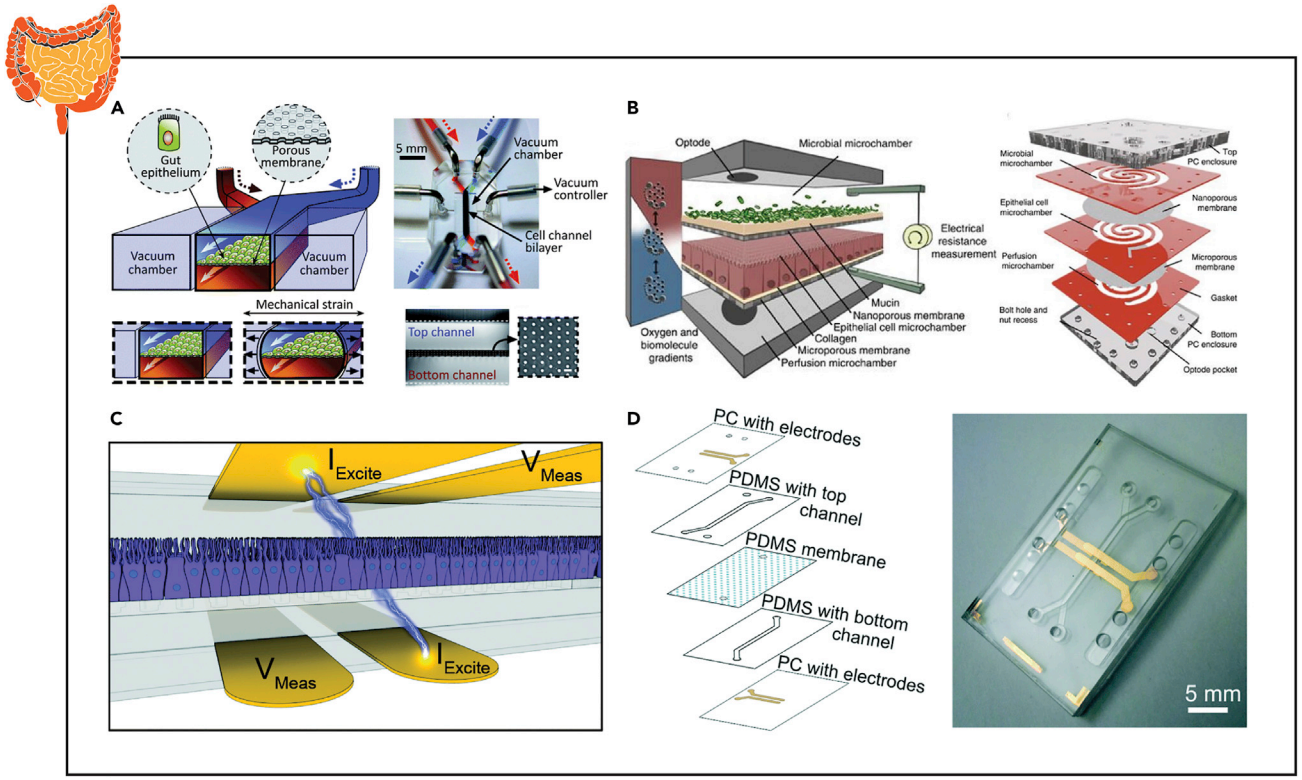

Figure 7. Examples of Instrumented Organ-on-chip Models of the Gut

(A) TEER measurements from a human Caco-2 intestinal epithelial cell monolayer exposed to microbial flora and intestinal peristalsis-like motions and flow via insertable wire electrodes.

(B) Gastrointestinal barrier integrity quantified in response to bacterial colonization in an anaerobic environment via chopstick style TEER electrodes.

(C and D) Intestinal monolayer barrier formation and villi differentiation assessed by measuring TEER and cell layer capacitance via integrated four-point impedance electrodes.

Reprinted and adapted with permission from: A (Kim et al., 2012); B (Shah et al., 2016); C (Henry et al., 2017); and D (van der Helm et al., 2019). TEER, transepithelial electrical resistance.

LUNG-ON-CHIP

Selective barrier function of airway epithelial cells in the lungs ensures the transport of oxygen from the air into the blood and prevents unwanted pathogens from entering the blood stream. Moreover, this tissue layer has and can be exploited as a route of administration for aerosolized drug compounds (Hittinger et al., 2017). Consequently, to develop these pharmacological screening platforms, it is critical to recapitulate the lung epithelial barrier integrity that is characteristic of the respiratory system. Walter et al. established an on-chip bilayer culture model with ports to insert commercial TEER electrodes to assess epithelial permeability (Figure 8A) (Walter et al., 2016). To confirm the feasibility of this model, lung epithelial A549 cells were cultured on a membrane within the device and exposed to a continuous fluidic flow for nutrient delivery. However, despite successful culture of a confluent cell monolayer and TEER values (46.4 $\pm$ 17.0 $\Omega.cm^2$) in concordance with data obtained from A549 cultures on Transwell inserts (27.8 $\pm$ 2.2 $\Omega.cm^2$), a respiratory air-liquid interface was not established. Toward better mimicking human physiology, Henry et al. cultured primary human airway epithelial cells in a microfluidic device with integrated gold electrodes for TEER and cell layer capacitance using 4-electrode impedance measurements, similar to designs discussed for gut chips above (Figure 8B) (Henry et al., 2017).

Although maintaining the air-liquid interface is critical for promoting differentiation and increasing barrier integrity, a coculture of airway epithelial cells with endothelial cells is needed to fully recapitulate the respiratory microenvironment (Sellgren et al., 2014). Skardal et al. established an air-liquid interface culture model on which layers of airway epithelial cells, airway stromal cells, and lung vascular endothelial cells were cultured on a semi-permeable membrane (Figure 8C) (Skardal et al., 2017). Barrier integrity and ion

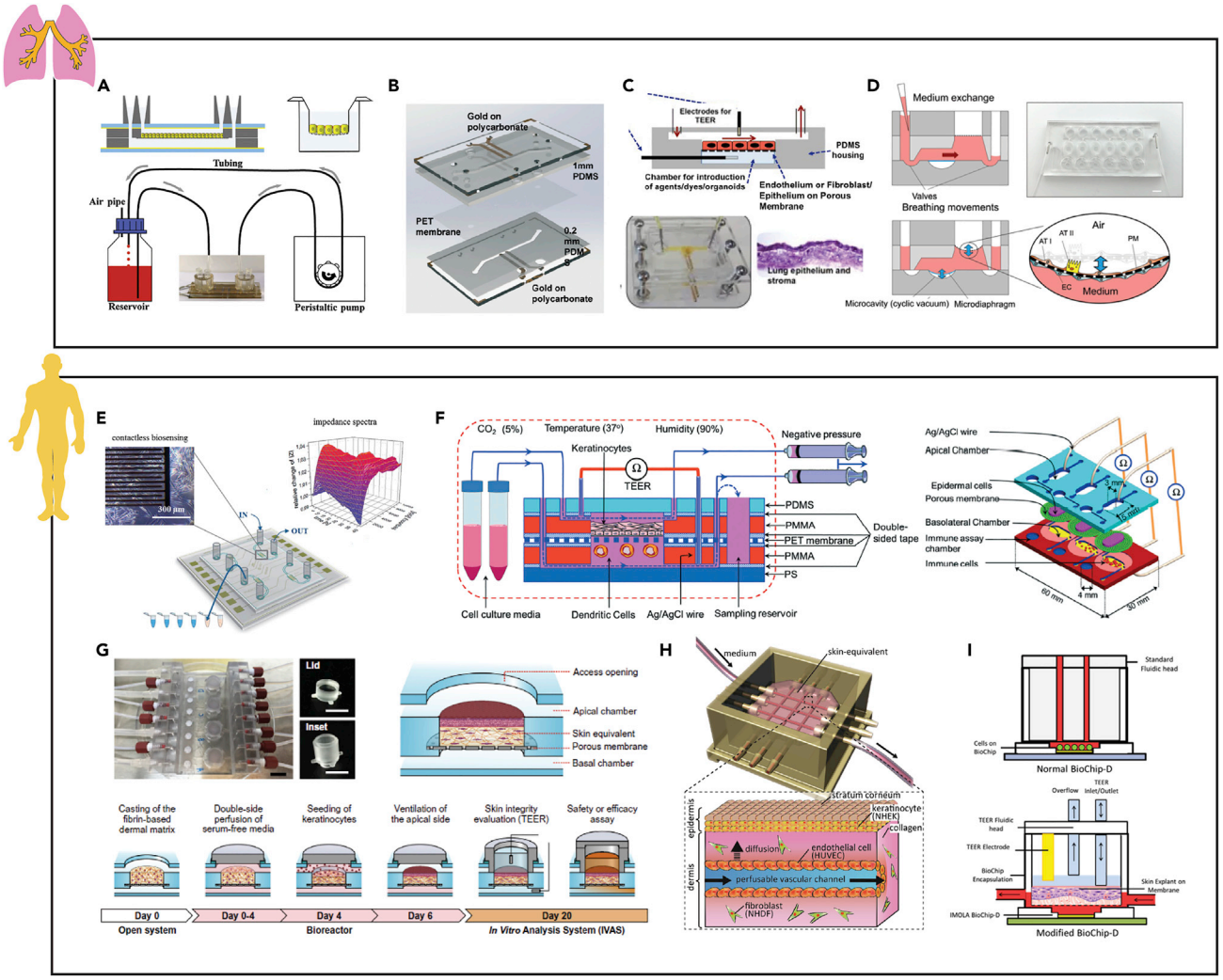

Figure 8. Examples of Instrumented Organ-on-chip Models of the Lungs and Skin

(A) Lung epithelial A549 cell tight junction integrity investigated within a bilayer chip with vasculature-like flow via TEER electrodes.

(B) Human airway epithelial cell mucociliary differentiation and barrier functionality quantified using capacitance and TEER measurements recorded overtime after establishing an air-liquid interface via integrated four-point impedance electrodes.

(C) Barrier integrity and chloride ion channel activity was assessed within an airway epithelial, stromal, and vascular endothelial cell coculture system via integrated TEER and short circuit current electrodes.

(D) Airway epithelial barrier permeability under physiological cyclic strain quantified via integrated TEER electrodes.

(E) Cell-substrate interactions, cell viability, and metabolic activity of foreskin-derived dermal fibroblasts in response to stimulation with circulating proinflammatory molecules quantified via interdigitated electrodes.

(F) Epidermal barrier functionality measured in response to skin allergens or physical stresses in a keratinocytes/immune cells coculture model via TEER electrodes.

(G) Barrier integrity of a full-thickness 3D human skin equivalent assessed via TEER electrodes.

(H) Capacitance of a vascularized 3D skin model measured via two electrodes was placed on either the dermal or the epidermal layers.

(I) Barrier stability, metabolic activity, and tissue breakdown measured simultaneously via TEER and extracellular acidification rate of L929 fibroblasts.

Reprinted and adapted with permission from: A (Walter et al., 2016); B (Henry et al., 2017); C (Skardal et al., 2017); D (Stucki et al., 2018); E (Charwat et al., 2014); F (Ramadan and Ting, 2016); G (Sriram et al., 2018); H (Mori et al., 2017); and I (Alexander et al., 2018). TEER, transepithelial electrical resistance.

channel activity was assessed using integrated TEER and short circuit current electrodes, respectively. Although TEER measures the overall permeability of a cell monolayer, short circuit current will exclusively measure ion transport through the cells in the monolayer by measuring the voltage with two electrodes placed near the epithelium and by injecting current with two separate electrodes placed in solution. Notably, the cystic fibrosis transmembrane conductance regulator (CFTR) chloride ion channel functionality is essential to regulate epithelial fluid transport. Therefore, electrophysiological sensing of the layered

lung model via short circuit current confirmed functionality of these chloride ion channels in response to CFTR agonist and antagonist. In addition to the physiological responses, cellular composition, and the air-liquid interface, mimicking the dynamic mechanical stimuli within lungs has been demonstrated to promote a biomimetic like phenotype *in vitro* (Huh et al., 2010). Stucki et al. developed a breathing on-chip lung model with integrated TEER electrodes and showed that epithelial barrier permeability was significantly affected by physiological cyclic strain (Figure 8D) (Stucki et al., 2018).

SKIN-ON-CHIP

The skin is the largest organ in the body containing several different cell types and organized into multiple layers, creating a strong barrier to the external environment (Van Gele et al., 2011). The epidermis, the outermost layer of the skin, is characterized by differentiated keratinocytes and the presence of an ortho-keratinized stratum corneum. Beneath the epidermis, the dermis contains hair follicles, sebaceous glands, nerve endings, and blood vessels and the subcutaneous layer, consisting of fat and connective tissues (Sung et al., 2019). To improve clinical dermatology and provide alternatives to animal cosmetic testing, *in vitro* skin equivalent models have been developed by coculturing heterogeneous populations. Charwat et al. established a non-invasive method to assess the health status of primary foreskin-derived dermal fibroblasts within a microfluidic cell culture device (Figure 8E) (Charwat et al., 2014). By integrating gold IDES, passivated with 300 nm Si_3N_4, onto chip for high-frequency (500 Hz–20 MHz) contactless spectroscopy, impedance changes in connective tissue corresponded to the application of circulating proinflammatory molecules. These higher testing frequencies were necessary to negate the influence of the passivation layer.

In addition to evaluating dermal health within these skin equivalent *in vitro* models, it is essential to recapitulate and quantify the critical role the skin plays in isolating the body from the external environment. Ramadan et al. developed a biomimetic organ-chip model to investigate how the immune system affects epidermal barrier integrity when exposed to skin allergens or physical stress (Figure 8F) (Ramadan and Ting, 2016). To mimic the immune component in the skin, a monolayer of immortalized human keratinocytes was established atop a porous membrane in the apical chamber on a bilayer chip and U937 immune cells cultured in the basolateral chamber of the same device. Further, an air-liquid interface was established while maintaining a continuous flow of nutrients to promote the keratinocyte differentiation and the development of a biomimetic stratum corneum. To confirm the integrity of this epidermal barrier, Ag/AgCl wire (0.5 mm) electrodes were inserted into predefined ports integrated into each device for measuring TEER with a Millicell ERS-2 Volt-Ohm Meter. As predicted, exposure to inert substances (lipopolysaccharides, cobalt sulfate, and glycerol) had no effect on TEER measurements, whereas skin allergens (nickel sulfate and dinitrochlorobenzene) and UV irradiation caused a decrease in TEER values.

In addition to the immune component in the skin, Sriram et al. developed a full-thickness 3D human skin equivalent by incorporating the dermal fibroblasts on-chip to recapitulate the connective tissues and vascular-like flow of dermal layers (Figure 8G) (Sriram et al., 2018). A human primary foreskin-derived dermal fibroblast laden poly(ethylene) glycol (PEG)-fibrinogen hydrogel was cross-linked atop a membrane to facilitate nutrient delivery from the basolateral channel. Immortalized human N/TERT-1 keratinocytes were then cultured atop this cell-laden hydrogel and allowed to differentiate to form a stratum corneum at the air-gel interface. To assess barrier functionality, Ag/AgCl TEER electrodes were inserted into the microfluidic device through designated ports. An increase in TEER values, in addition to a decrease in small molecule permeability, confirmed that barrier integrity was significantly higher under perfusion, indicating the importance of dermal vasculature. Therefore, to better recapitulate the dermal microenvironment, Mori et al. developed a vascularized *in vitro* model of the skin by coculturing human epidermal keratinocytes monolayer atop a human dermal fibroblast-laden collagen-based hydrogel with a perfusable vascular channel containing human umbilical vein endothelial cells (Figure 8H) (Mori et al., 2017). In this work, capacitance was measured with a Sanwa Electric LCR meter (calculated from impedance) to demonstrate the barrier function of the perfused skin equivalent. To measure capacitance within the microfluidic model, two electrodes were carefully placed either on the dermal or on the epidermal layers at the air-liquid interface. Using this method, capacitance of the epidermal layer was found to significantly lower than that of the dermal layer.

Although epidermal barrier integrity is a critical metric for understanding the skin, dermal toxicity is also affected by the acidification of the extracellular microenvironment. Alexander et al. developed an

integrated MPS for automated monitoring and TEER acquisition based on an intelligent mobile laboratory for *in vitro* diagnostics to quantify extracellular acidification rate (Figure 8I) (Alexander et al., 2018). This automated system was capable of fluid handling for maintaining an air-liquid interface and perfusing PBS for TEER measurements. The simultaneous TEER and acidification rate measurement of L929 fibroblasts in response to sodium dodecyl sulfate medium on-chip demonstrated the ability to both monitor barrier stability, metabolic activity, and tissue breakdown over time.

LIVER-ON-CHIP

The liver is a vital organ for filtering toxins from the blood. Its inclusion in models is crucial for pharmaceutical screening to determine both drug metabolism and toxicity (Hughes et al., 2017). As such, *in vitro* models which aim to better recapitulate the human liver system offer potential gains toward therapeutic development in both the liver and systemic homeostasis. Improvements in fundamental biology, materials, and techniques aim to enable 3D systems such as liver-on-chips to more successfully recapitulate the system. Given the importance of the liver as well as the breadth of functions, several types of sensor technologies (e.g. aptameric, fluorescent, electrochemical, and luminescence sensors; Figure 2) have emerged and been demonstrated in liver microfluidic chips. Utilizing surface modifications and bio polymers in conjunction with common electrode testing configurations (i.e., cyclic voltammetry [CV], EIS), real-time measures of analyte concentration can be achieved. With the breadth of the field, one example of several types of sensors are summarized below.

Aptamer-based electrochemical sensors function by serving as high-affinity protein ligands for the detection of adsorption of an analyte via a change in redox properties of an electrode (Kirby et al., 2004; Zhou et al., 2015). For the liver, Zhou et al. developed an aptamer sensor for transforming growth factor (TGF)-β1 (Figure 9A). The device comprised of a 3 × 4 gold, individually addressable electrode array (475 μm × 150 μm) and was connected to a potentiostat to run square wave voltammetry. The device was utilized to measure the concentration via percent signal suppression hourly in a liver-chip containing both hepatocytes and stellate cells, allowing a better understanding of the cross-talk between the two cell types in response to alcohol exposure. With COMSOL numerical modeling software, a diffusion-reaction model was utilized to validate the concentration measurements. This work was continued by using a fluorescent-bead-based optical sensors instead to again measure TGF-β1 on chip, which now included specific sensing channels separated from culture chambers by a hydrogel (Figure 9B) (Son et al., 2017). The sensor system operated by the desired protein(s) diffusing from a microfluidic culture chamber (1.5 mm width) containing cultured hepatocytes into the adjacent sensing channel (0.25 mm width) via a PEG hydrogel barrier formed by two columns of PDMS posts (80 μm each), which prevented cells from entering the sensing channel. The sensing channel contained antibody (ab)-coated capture (non-fluorescent, streptavidin-coated polystyrene particles 5–5.9 μm diameter) and detection beads (fluorescent, streptavidin-coated polystyrene particles 5–5.9 μm diameter). The introduction of the protein(s) of interest caused aggregation of the fluorescent particles, which could be measured with a fluorescent microscope. Following detection of fluorescence above a standard threshold, the intensity was quantified. Discrete sensing channels enabled the flexibility to replenish and replace the beads as desired prior to saturation. In addition, the group was able to demonstrate a multiplexing capability with both TGF-β1 and hepatocyte growth factor simultaneously using multiple sets of beads with different fluorescent markers.

Immune-based electrochemical sensing in a liver microfluidic chip has been demonstrated using both bead- (Figure 9C) (Riahi et al., 2016) and electrode-based (Shin et al., 2017) platforms. Shin et al., measuring once daily, developed a set of three antibody-coated electrodes (Au working and counter electrodes and Ag reference electrode) for detecting human albumin and glutathione-S-transferase-alpha (GST-α). Electrochemical impedance spectroscopy (EIS) was utilized to measure the changes in impedance upon binding of the protein(s). This approach was validated with ELISA. Following saturation, the group demonstrated a cleaning procedure that was conducted 25 times without significant loss in sensitivity. With the use of on-chip microfluidic valves, they were able to enable their semi-batch sensor to be used continuously.

Bavli et al. developed a holistic determination of mitochondrial function in a liver chip system using a combination of a luminescence and enzyme-based sensors to measure oxygen and glucose/lactose (Figure 9D) (Bavli et al., 2016). The lifetime-based luminescence-quenching sensor measured oxygen by observing the change in phosphorescence decay time of ruthenium-phenanthroline-based phosphorescence dye in the

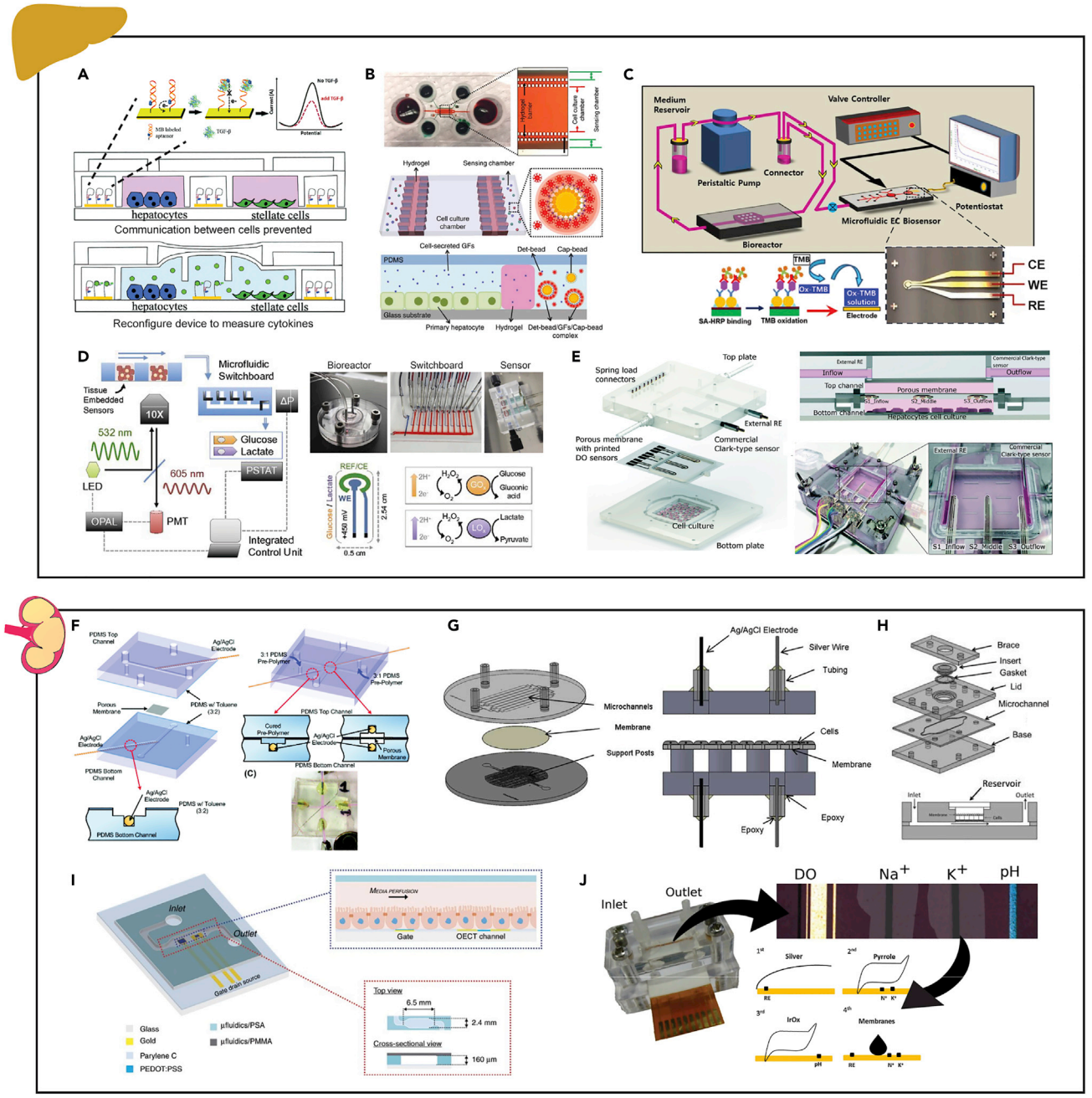

Figure 9. Examples of Instrumented Organ-on-chip Models of the Liver and Kidneys

(A) Detection of TGF-β1 within a reconfigurable device to allow communication between injured hepatocytes and stellate cells via an aptamer-based electrochemical sensor.

(B) On-chip detection of the hepatocyte growth factor and TGF-β1 secreted by primary hepatocytes via a fluorescent-bead-based optical sensor.

(C) Transferrin and albumin production from human primary hepatocytes cultured in the bioreactor quantified via a bead-based electrochemical immunosensor.

(D) Continuous real-time monitoring of hepatocyte metabolic function via a glucose/lactate enzyme-based electrochemical sensors and oxygen sensing phosphorescent microprobes.

(E) Hepatocyte oxygen consumption rate assessed via inkjet-printed electrochemical dissolved oxygen sensors and commercial Clark-type sensors.

(F) Permeability study of an MDCK-2 cell monolayer cultured on the membrane of a bilayer chip via TEER electrodes.

(G) Assessment of renal epithelial cell growth and tight junction integrity quantified within a continuous fluid shear stress model via integrated TEER electrodes.

(H) TEER measurements from a human renal epithelial cell monolayer cultured in a multi-use microfluidic device with integrated electrodes.

Figure 9. *Continued*

(I) Electrical cell–substrate impedance monitoring of MDCK-2 cells to investigate wound healing and barrier integrity via an organic electrochemical transistor.

(J) Electrochemical measurement of dissolved oxygen, Na^+ and K^+ ion concentration, and pH in kidney exactments via potentiometric and amperometric electrodes.

Reprinted and adapted with permission from: A (Zhou et al., 2015); B (Son et al., 2017); C (Riahi et al., 2016); D (Bavli et al., 2016); E (Moya et al., 2018b); F (Douville et al., 2010); G (Ferrell et al., 2010); H (Brakeman et al., 2016); I (Curto et al., 2017); and J (Moya et al., 2018a). TGF-β1, transforming growth factor; MDCK-2, Madin Darby canine kidney-2; TEER, transepithelial electrical resistance.

presence of varying amounts of oxygen. Lactose and glucose were measured using glucose oxidase and lactose oxidase, which both released a proportional level of hydrogen peroxide that could be detected by polarized platinum electrodes as part of a commercially available amperometric system measured using a potentiostat. Combined, these metrics indicated the transition of the mitochondria from aerobic to anaerobic metabolism, which preceded cell death from exposure to rotenone and troglitazone. Critically, the team demonstrated that per the Warburg effect, all three measurements (oxygen, glucose, and lactose) were required to witness changes in mitochondrial function.

Using an inkjet printer, Moya et al. demonstrated the capability to print a set of three electrodes (Au: working and counter electrodes; Ag/AgCl: reference electrode) as a dissolved oxygen sensor directly into a microfluidic chip's membrane (Figure 9E) (Moya et al., 2018b). The sensors were validated using commercial Clark-type sensors and oriented to measure a gradient across the cell culture (via cyclic voltammetry) that was demonstrated in both human and rodent hepatocytes.

KIDNEY-ON-CHIP

The kidneys are responsible for removing waste, maintaining water and salt homeostasis, and clearing spent drug compounds. Therefore, electrochemical sensors offer great potential for monitoring renal function. However, certain chemotherapeutic and antiviral pharmacotherapies can cause nephrotoxicity, which significantly reduces their efficacy (Wilmer et al., 2016). To understand the molecular mechanisms of drug-induced kidney toxicity and better predict drug efficacy during the drug discovery process, researchers have developed *in vitro* models that recapitulate critical aspects of kidney architecture. The kidneys are a highly vascularized organ that contains more than 10 district types of renal cells that are organized within a complex 3D ECM environment (Wilmer et al., 2016). Although the complex 3D architecture of a nephron has not yet been replicated *in vitro*, kidney-on-chip models that mimic the vasculature-like flow have a positive effect on renal cell phenotype (Huang et al., 2014; Peloso et al., 2015). Specifically, the organization of cytoskeleton and the integrity of junctional complexes, in addition to gene, protein, and receptor expression, are affected by fluidic flow (Essig et al., 2001; Jang et al., 2013).

Conventional analytical methods used to validate the kidney-on-chip models and assess nephrotoxicity of pharmacological compounds require manual sample collection and laborious post-process analysis. To overcome these analytical challenges, Douville et al. developed a two-layer PDMS-based microfluidic device with integrated Ag/AgCl electrodes for real-time TEER measurements in the absence of fluid flow (Figure 9F) (Douville et al., 2010). TEER can be used to assess tight junctions needed to maintain volume balance and fluid composition in the body (Massry and Glassock, 2001). Confirming that TEER can be used to assess renal barrier integrity, Douville et al. demonstrated that Madin Darby Canine Kidney (MDCK-2) cells grown in static conditions exhibited higher TEER values than cells not expected to form tight junctions (C2C12) on-chip (Douville et al., 2010). Further, the disruption of barrier integrity with TritonX-100 also resulted in a significant decrease in paracellular resistance. That same year, Ferrell et al. demonstrated that TEER can also be used to assess cell growth and cell-cell junction integrity of human renal epithelial cells in addition to MDCK cells (Figure 9G) (Ferrell et al., 2010). In conjunction with TEER quantification, shear-dependent changes (~1 dyn/cm^2) on cytoskeletal F-actin expression were assessed on-chip via immunofluorescent staining. As a proof-of-concept, TEER was confirmed with a Ca^{2+} switch technique to increase insulin transport and decrease in TEER. Brakeman et al. later improved upon these continuous fluid shear stress models with integrated electrodes for TEER by fabricating a device that could be used by multiple iterations (Figure 9H) (Brakeman et al., 2016). In contrast to conventional designs, a multi-use device enables increased throughput with minimal fabrication requirements. Moreover, establishing a confluent renal epithelium commonly takes several days, which limits experiment turn-around time. Therefore, this modular microfluidic system that uses commercially available

Transwell inserts can increase the total number of experimental trials, in addition to being used to assess physiological flow conditions.

In addition to barrier integrity, receptor expression and cell volume and its regulation are key factors in kidney cell function and pathogenesis (Cho et al., 2016; Vala et al., 2013). Fluorescence microscopy can be used to non-destructively monitor nephrotoxicity within organ-chip models. Cho et al. established a kidney-on-chip model with real-time quantification of immunocaptured nanoparticles with light scatting to assess the toxicity of a known nephrotoxicant, cisplatin (Cho et al., 2016). In response to kidney toxicants, γ-glutamyl transpeptidase (GGT) is released into the tubular lumen and therefore provides a target to assess toxicity. Consequently, it was confirmed that dosing renal adenocarcinoma cells with cisplatin results in the immonoagglutination of anti-GGT conjugated fluorescent nanoparticles. The increased signal caused by the clumping of these fluorescent nanoparticles was detectable in real-time with any readily available smartphone camera.

Toward understanding the ability of these *in vitro* kidney models to regulate the transport of ions and various organic molecules, in-line sensors must be developed and integrated on-chip. Curto et al. designed an organic electrochemical transistor (three terminal devices made of PEDOT:PSS) to monitor wound-healing and toxicity in a microfluidic system with canine kidney cells (Figure 9I) (Curto et al., 2017). To establish a wound-healing assay, MDCK-2 cells grown on the sensors were wounded by shorting the transistor. The injury resulted in a complete loss of cell-related impedance that continuously increased to 1.5-fold higher than the preinjury model as cells recovered. To demonstrate the added benefit of using an organic electrochemical transistor for drug toxicity monitoring, cells were treated with Cyt D to disrupt their actin filaments. Unlike more traditional metallic electrodes, organic electrodes are easily processed, chemically tunable, and biocompatible (Khodagholy et al., 2012; Strakosas et al., 2014, 2016). Using their instrumented model, Cyt D resulted in a decrease in cell-related impedance and could then recover barrier integrity by perfusing the device with fresh medium, thereby further demonstrating the utility of an in-line monitoring system (Curto et al., 2017).

Although not yet integrated into an organ-chip model, Moya et al. developed highly sensitive, low-volume electrochemical sensors for measuring the dissolved oxygen, Na^+ and K^+ ion concentration, and pH in kidney exactments (Figure 9J) (Moya et al., 2018a). Dissolved oxygen was measured amperometrically with three electrodes, ion concentrations were measured potentiometrically with ion-sensitive electrodes, and pH was measured potentiometrically with iridium oxide–coated electrodes. As a proof-of-concept for using electrochemical sensors within *in vitro* kidney models, the urine of mice on different diets was assessed. Although dissolved oxygen in urine is not a relevant physiological parameter, oxygen control is essential for cell cultures systems. Further, despite urine often being available in large volumes, electrochemical sensors only required 0.83μL for high sensitivity, making them well suited for integration within microfluidic culture models.

Surface plasmon resonance (SPR) sensors are efficient tools for real-time and label-free quantification of changes in cell volume and shape (Robelek and Wegener, 2010). Vala et al. reports that changes in normal rat kidney epithelial cell size in response to osmotic stress may be assessed using SPR (Vala et al., 2013). However, SPR has not yet been implemented within a kidney-on-chip model and therefore represents a future approach for improved on-chip quantitation of kidney toxicity.

CANCER-ON-CHIP

Despite improved surgical and pharmacological treatments targeting the primary tumor, metastasis remains responsible for more than 90% of cancer-associated mortality (Chaffer and Weinberg, 2011). Due to discrepancies between cell behavior *in vitro* and *in vivo*, engineered 3D culture models may offer means to better mimic the extracellular matrix (ECM) (Even-Ram and Yamada, 2005). Consequently, organ-chip models have been developed to recapitulate the 3D *in vivo* tumor microenvironment *in vitro* to investigate the metastatic processes (Portillo-Lara and Annabi, 2016). Most commonly, these cell migration assays are based on the Boyden chamber assay, in which cancerous cells are cultured atop an ECM-coated membrane, and cell invasion is visually quantified as cells move through the matrix (Chen, 2005). However, conventional methodologies for evaluating cell migration within these assays often rely on endpoint and label-based microscopy.

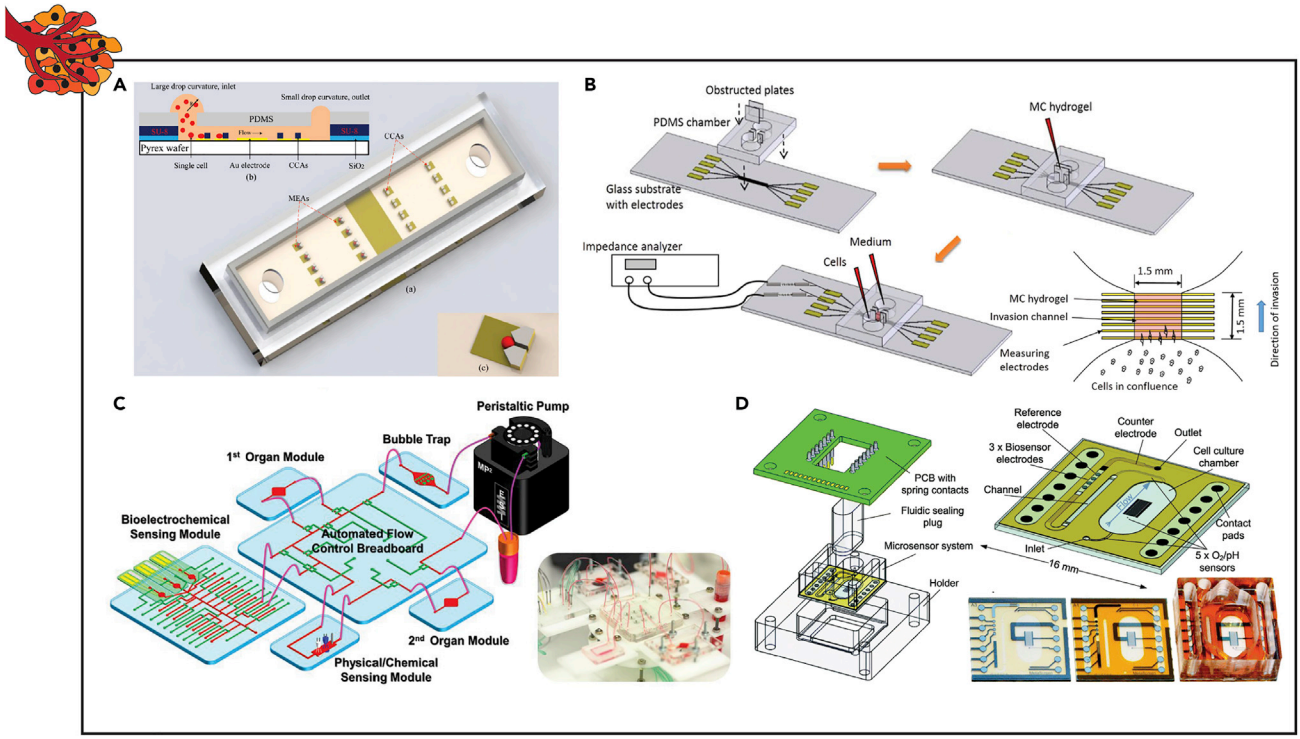

Figure 10. Examples of Instrumented Organ-on-chip Models of Cancer

(A) Electrical cell–substrate impedance sensing to monitor cancer cell metastasis via an electrode array.

(B) Malignant cell invasion quantified in response to biomimetic cytokine stimulation via interdigitated electrodes.

(C) Oxygen concentration, biochemical profiles, temperature, and pH changes resulting from cancer and its treatment quantified by plumbing together biochemical, physical, and chemical sensing modules.

(D) Monitoring T98G human brain cancer cells metabolism within a single device via miniaturized pH and oxygen electrodes and amperometric biosensors for glucose, lactate, and peroxide.

Reprinted and adapted with permission from: A (Nguyen et al., 2013); B (Lei et al., 2016); C (Zhang et al., 2017); D (Weltin et al., 2013).

Although microscopy may provide a semiquantitative analysis of metastasis, the process is almost always labor intensive, prone to inconsistent results, and often fails to capture the onset and rate of invasion and migration (Bird and Kirstein, 2009). To overcome these limitations, the use of impedance-based technologies has allowed the development of kinetic-cell response profiles using the Boyden chamber assay (Bird and Kirstein, 2009). Despite the advantages of electrical cell–substrate impedance sensing (ECIS) within this model, the Boyden chamber assay has inherent limitations. Both the pore size of the membrane and the effects of gravity may highly influence the number and rate at which cells invade (Lei et al., 2016). To overcome these limitations while incorporating the benefits of impedance spectroscopy for monitoring cell migration, Nguyen et al. reports on the development and characterization of an MPS with integrated ECIS (Figure 10A) (Nguyen et al., 2013). Moreover, in addition to a microelectrode array (MEA) and microfluidic channel, these sensor chips contained a cell capture array layer for single-cell analysis, which may provide unique insights into heterogeneous cell behavior (Levsky and Singer, 2003). In this study, migration of single metastatic MDA-MB-231 cells was demonstrated in real-time with a rapid change (~10 Ω/s) in impedance magnitude, with no prominent impedance change for less-metastatic MCF-7 cells (Nguyen et al., 2013). This combinatorial approach integrating ECIS within an MPS enables a more rapid, higher-resolution, and real-time quantification of cell migration kinetics compared with previous methodologies to quantify metastasis (Bird and Kirstein, 2009; Chaw et al., 2007; Chen, 2005; Nguyen et al., 2013). Utilizing a similar ECIS-based MPS, Lei et al. investigated the effects of biomimetic cytokine stimulation and cell invasion (Figure 10B) (Lei et al., 2016). Specifically, by fabricating an MPS with eight 100 μm electrodes spaced 100 μm apart, Lei et al. was able to calculate the rate of cell migration and demonstrated that with increasing concentrations of IL-6, the rate at which malignant BPC-BM1 cells migrate increased.

Similarly, while cytokine stimulation from neighboring cells increases the rate of malignancy (Johnson et al., 2012), the extracellular manipulation of the tumor microenvironment by cancer cell populations may also promote cancer metastasis (Jiang, 2017; Kato et al., 2013; Muz et al., 2015). Toward understanding these modified environments and their effect on cellular metabolism and metastatic processes, changes in oxygen concentration, biochemical profiles, temperature, and pH levels have been analyzed using microfluidic devices. For example, Zhang et al. engineered a multi-organ, multi-sensor MPS to investigate how liver cancer and its treatment affects cardiovascular health (Figure 10C) (Zhang et al., 2017). By plumbing together sensors for pH, temperature, oxygen, and cardiac and liver biomarkers, the authors confirmed their cancer-on-chip model accurately mimicked the anticancer efficacy of doxorubicin. As an alternative to plumbing multiple systems together, which is both technically challenging and increases the risk of failure, miniaturized biosensors were integrated into a single device to monitor T98G human brain cancer cell metabolism (Figure 10D) (Weltin et al., 2013). More importantly, this multiparametric microfluidic device maintained a highly effective medium change at low flow rates (2 μL/min) and low-volume (15 μL), thereby enabling finely controlled drug exposure with limited sample availability, while also limiting shear stress.

CONCLUSIONS AND FUTURE DIRECTIONS

Advances in bioengineering and microfabrication technologies have made it possible to significantly improve traditional 2D culture models and study cells alongside physiologically relevant factors such as heterogeneous cell interfaces (Kim et al., 2012), chemical gradients (Kim et al., 2011), and mechanical cues (Douville et al., 2011; Jang et al., 2011; Kim et al., 2012), or in heterogeneous 3D organoids (Sato and Clevers, 2013). Recent work has demonstrated the presence of spontaneous neural activity of human midbrain organoids recorded on a 16-channel microelectrode array (Monzel et al., 2017). The further development of high-density MEAs (Lonardoni et al., 2019) will improve the resolution of cell activity measurement, possibly down to individual ion channels, thus providing a larger footprint of recording area to evaluate network dynamics and enable further multiplexing of sensor types. Specifically, for understanding cognitive function, the increased recording area could be used for coculturing different neuronal populations (e.g., thalamus–cortex; hippocampus–cortex) and studying interaction between the two segregated sub-networks. Additionally, while individual cells can be identified by discrete AP waveforms with conventional techniques, understanding the network dynamics of heterogeneous cultures on chip, such as in heterogeneous and hierarchical neural tissue, will require new multiplexed sensor designs to distinguish excitatory vs inhibitory neurons as well as unique phenotypes via neurotransmitter profiling.

Multiplexing different sensor modalities into chip platforms will be crucial for developing multi-organ MPS. To date, a handful of instrumented multi-organ MPS have been demonstrated. The 'physiome-on-a-chip' utilizes interconnected Transwells to recapitulate up to 10 different organ systems, while monitoring gut TEER values (Edington et al., 2018). Further, this platform has been leveraged to study the role of inflammation and products of the microbiome in gut-liver-related diseases such as ulcerative colitis (Trapecar et al., 2019). Miller and Shuler have developed a pumpless, non PDMS MPS that recapitulates 13 organs (Miller and Shuler, 2016). However, the system relies on microscopy or endpoint measures of cell function. At the forefront of MPS and multiplexed sensing technologies, Oleaga et al. has engineered a human, four-organ MPS with a pair of MEAs and laser-deflection cantilever systems to monitor motor neuron, CM, skeletal muscle, and liver interactions (Oleaga et al., 2018, 2019).

On potential future direction, endogenous electric fields play an important role in development and wound repair of endothelial and epithelial tissues, providing guidance cues for progenitor cells. MPS platforms are amenable to the applications of DC electric fields while utilizing measures of bioimpedance to assess tissue maturation and therefore may be beneficial in establishing fundamental principles of development and wound healing in peripheral nerve, skin, and vasculature.

A key advantage beyond the use of human tissue from iPSC sourcing is the opportunity to incorporate electronic-based sensors and stimulation tools for real-time interrogation of cell function. As part of this review, we have highlighted some of the work on the forefront of these technologies, covering both active and passive sensor technologies to measure cell activity from membrane depolarization to analyte concentrations (Figure 2). The incorporation of new innovations in organic electronics, aptamer/immune ligands, microfluidics, and sensing protocols (i.e., high frequency impedance spectroscopy) will drive the use of these platforms from the academic laboratory to commercial use. Further, the complexity of organ-chips

will be greatly improved by the convergence of MPS and additive fabrication techniques including 3D tissue printing with cell-laden bioinks. Although fabrication methods are outside the scope of this review, a detailed prospective has been written by Parrish et al. (Parrish et al., 2019).

Altogether, MPS research has produced systems capable of recapitulating aspects of disease and tissue models. Continued integration of these models with electrical sensors offers the ability to elucidate changes to cellular function and signaling with finite control of the environment. Further study utilizing these systems offers scientists a potentially high-throughput tool to ask basic biological questions toward understanding life and its diseases. Therefore, instrumented benchtop models of human tissue that recapitulate the heterogeneity and architecture of organ tissue offer great potential for disrupting the pharmaceutical pipeline and fundamental research.

ACKNOWLEDGMENTS

This work was supported by American Heart Association (AHA) Grant #19PRE34430181 (J.R. Soucy). R.A. Koppes and A.N. Koppes acknowledge the support from the National Institutes of Health (NIH, R21EB025395-01) and the Department of Chemical Engineering, College of Engineering at Northeastern University.

AUTHOR CONTRIBUTIONS

J.R.S. and R.A.K. outlined the manuscript. J.R.S. prepared the figures. J.R.S, A.J.B, and R.A.K. wrote the manuscript. All authors edited and provided feedback on the manuscript. R.A.K. and A.N.K. supervised the work.

REFERENCES

Abassi, Y.A., Xi, B., Li, N., Ouyang, W., Seiler, A., Watzele, M., Kettenhofen, R., Bohlen, H., Ehlich, A., Kolossov, E., et al. (2012). Dynamic monitoring of beating periodicity of stem cell-derived cardiomyocytes as a predictive tool for preclinical safety assessment. Br. J. Pharmacol. *165*, 1424–1441.

Agarwal, A., Goss, J., Cho, A., McCain, M., and Parker, K. (2013). Microfluidic heart on a chip for higher throughput pharmacological studies. Lab Chip *13*, 3599–3608.

Alexander, F.A., Eggert, S., and Wiest, J. (2018). Skin-on-a-Chip: transepithelial electrical resistance and extracellular acidification measurements through an automated air-liquid interface. Genes (Basel) *9*, https://doi.org/10.3390/genes9020114.

Anava, S., Greenbaum, A., Ben Jacob, E., Hanein, Y., and Ayali, A. (2009). The regulative role of neurite mechanical tension in network development. Biophys. J. *96*, 1661–1670.

Aung, A., Bhullar, I., Theprungsirikul, J., Davey, S., Lim, H., Chiu, Y.-J., Ma, X., Dewan, S., Lo, Y.-H., McCulloch, A., et al. (2015). 3D cardiac μtissues within a microfluidic device with real-time contractile stress readout. Lab Chip *16*, 153–162.

Bank, I.E.M., Timmers, L., Gijsberts, C.M., Zhang, Y.-N., Mosterd, A., Wang, J.-W., Chan, M.Y., Hoog, V., Lim, S., Sze, S., et al. (2015). The diagnostic and prognostic potential of plasma extracellular vesicles for cardiovascular disease. Expert Rev. Mol. Diagn. *15*, 1577–1588.

Barizuddin, S., Liu, X., Mathai, J.C., Hossain, M., Kevin, G.D., and Gangopadhyay, S. (2010). Automated targeting of cells to electrochemical electrodes using a surface chemistry approach for the measurement of quantal exocytosis. ACS Chem. Neurosci. *1*, 590–597.

Bavli, D., Prill, S., Ezra, E., Levy, G., Cohen, M., Vinken, M., Vanfleteren, J., Jaeger, M., and Nahmias, Y. (2016). Real-time monitoring of metabolic function in liver-on-chip microdevices tracks the dynamics of mitochondrial dysfunction. Proc. Natl. Acad. Sci. U S A *113*, E2231–E2240.

Bein, A., Shin, W., Jalili-Firoozinezhad, S., Park, M.H., Sontheimer-Phelps, A., Tovaglieri, A., Chalkiadaki, A., Kim, H.J., and Ingber, D.E. (2018). Microfluidic organ-on-a-chip models of human intestine. Cell. Mol. Gastroenterol. Hepatol. *5*, 659–668.

Bhatia, S.N., and Ingber, D.E. (2014). Microfluidic organs-on-chips. Nat. Biotechnol. *32*, 760–772.

Bird, C., and Kirstein, S. (2009). Real-time, label-free monitoring of cellular invasion and migration with the xCELLigence system. Nat. Methods *6*, 622.

Booth, R., and Kim, H. (2012). Characterization of a microfluidic in vitro model of the blood-brain barrier (muBBB). Lab Chip *12*, 1784–1792.

Booth, R., and Kim, H. (2014). Permeability analysis of neuroactive drugs through a dynamic microfluidic in vitro blood–brain barrier model. Ann. Biomed. Eng. *42*, 2379–2391.

Boudou, T., Legant, W.R., Mu, A., Borochin, M.A., Thavandiran, N., Radisic, M., Zandstra, P.W., Epstein, J.A., Margulies, K.B., and Chen, C.S. (2012). A microfabricated platform to measure and manipulate the mechanics of engineered cardiac microtissues. Tissue Eng.Part A *18*, 910–919.

Bowen, A.L., and Martin, S.R. (2010). Integration of on-chip peristaltic pumps and injection valves with microchip electrophoresis and electrochemical detection. Electrophoresis *31*, 2534–2540.

Braam, S.R., Tertoolen, L., van de Stolpe, A., Meyer, T., Passier, R., and Mummery, C.L. (2010). Prediction of drug-induced cardiotoxicity using human embryonic stem cell-derived cardiomyocytes. Stem Cell Res. *4*, 107–116.

Brakeman, P., Miao, S., Cheng, J., Lee, C.-Z., Roy, S., Fissell, W.H., and Ferrell, N. (2016). A modular microfluidic bioreactor with improved throughput for evaluation of polarized renal epithelial cells. Biomicrofluidics *10*, 64106.

Bresadola, M. (1998). Medicine and science in the life of Luigi Galvani (1737-1798). Brain Res.Bull. *46*, 367–380.

Brown, J.A., Codreanu, S.G., Shi, M., Sherrod, S.D., Markov, D.A., Neely, M.D., Britt, C.M., Hoilett, O.S., Reiserer, R.S., Samson, P.C., et al. (2016). Metabolic consequences of inflammatory disruption of the blood-brain barrier in an organ-on-chip model of the human neurovascular unit. J. Neuroinflammation *13*, 306.

Brown, J.A., Pensabene, V., Markov, D.A., Allwardt, V., Neely, M.D., Shi, M., Britt, C.M., Hoilett, O.S., Yang, Q., Brewer, B.M., et al. (2015). Recreating blood-brain barrier physiology and structure on chip: a novel neurovascular microfluidic bioreactor. Biomicrofluidics *9*, https://doi.org/10.1063/1.4934713.

Buehler, S.M., Stubbe, M., Gimsa, U., Baumann, W., and Gimsa, J. (2011). A decrease of intracellular ATP is compensated by increased respiration and acidification at sub-lethal parathion concentrations in murine embryonic neuronal cells: measurements in metabolic cell-culture chips. Toxicol. Lett. *207*, 182–190.

Butler, M.I., Cryan, J.F., and Dinan, T.G. (2019). Man and the microbiome: a new theory of everything? Annu. Rev. Clin. Psychol. *15*, 371–398.

Byku, M., and Mann, D.L. (2016). Neuromodulation of the failing heart: lost in translation? JACC Basic Transl. Sci. *1*, 95–106.

Caspi, O., Itzhaki, I., Kehat, I., Gepstein, A., Arbel, G., Huber, I., Satin, J., and Gepstein, L. (2009). In Vitro electrophysiological drug testing using human embryonic stem cell derived cardiomyocytes. Stem Cells Dev. *18*, 161–172.

Chaffer, C.L., and Weinberg, R.A. (2011). A perspective on cancer cell metastasis. Science *331*, 1559–1564.

Charwat, V., Joksch, M., Sticker, D., Purtscher, M., Rothbauer, M., and Ertl, P. (2014). Monitoring cellular stress responses using integrated high-frequency impedance spectroscopy and time-resolved ELISA. Analyst *139*, 5271–5282.

Chaw, K.C., Manimaran, M., Tay, F.E.H., and Swaminathan, S. (2007). Matrigel coated polydimethylsiloxane based microfluidic devices for studying metastatic and non-metastatic cancer cell invasion and migration. Biomed. Microdevices *9*, 597–602.

Chen, H.-C.C. (2005). Boyden chamber assay. Methods Mol. Biol. *294*, 15–22.

Chen, L., Ilham, S.J., Guo, T., Emadi, S., and Feng, B. (2017). In vitro multichannel single-unit recordings of action potentials from mouse sciatic nerve. Biomed. Phys. Eng. Express *3*, https://doi.org/10.1088/2057-1976/aa7efa.

Cheng, W., Klauke, N., Smith, G., and Cooper, J.M. (2010). Microfluidic cell arrays for metabolic monitoring of stimulated cardiomyocytes. Electrophoresis *31*, 1405–1413.

Cho, S., Islas-Robles, A., Nicolini, A.M., Monks, T.J., and Yoon, J.-Y. (2016). In situ, dual-mode monitoring of organ-on-a-chip with smartphone-based fluorescence microscope. Biosens. Bioelectron. *86*, 697–705.

Cimetta, E., Godier-Furnémont, A., and Vunjak-Novakovic, G. (2013). Bioengineering heart tissue for in vitro testing. Curr. Opin. Biotechnol. *24*, 926–932.

Currie, K.P.M. (2010). Inhibition of Ca2+ channels and adrenal catecholamine release by G protein coupled receptors. Cell. Mol. Neurobiol. *30*, 1201–1208.

Curto, V.F., Marchiori, B., Hama, A., Pappa, A.M., Ferro, M.P., Braendlein, M., Rivnay, J., Fiocchi, M., Malliaras, G.G., Ramuz, M., et al. (2017). Organic transistor platform with integrated microfluidics for in-line multi-parametric in vitro cell monitoring. Microsyst. Nanoeng. *3*, 17028.

de Diego, A.M. (2010). Electrophysiological and morphological features underlying neurotransmission efficacy at the splanchnic nerve-chromaffin cell synapse of bovine adrenal medulla. Am. J. Physiol.Cell Physiol. *298*, C397–C405.

de Diego, A.M.G., Gandia, L., and Garcia, A.G. (2008). A physiological view of the central and peripheral mechanisms that regulate the release of catecholamines at the adrenal medulla. Acta Physiol. *192*, 287–301.

Denning, C., Borgdorff, V., Crutchley, J., Firth, K.S., George, V., Kalra, S., Kondrashov, A., Hoang, M.D., Mosqueira, D., Patel, A., et al. (2016). Cardiomyocytes from human pluripotent stem cells: from laboratory curiosity to industrial biomedical platform. Biochim Biophys Acta *1863*, 1728–1748.

Deosarkar, S.P., Prabhakarpandian, B., Wang, B., Sheffield, J.B., Krynska, B., and Kiani, M.F. (2015). A novel dynamic neonatal blood-brain barrier on a chip. PLoS One *10*, e0142725.

Dittami, G.M., and Rabbitt, R.D. (2009). Electrically evoking and electrochemically resolving quantal release on a microchip. Lab Chip *10*, 30–35.

Douville, N.J., Tung, Y.-C., Li, R., Wang, J.D., El-Sayed, M., and Takayama, S. (2010). Fabrication of two-layered channel system with embedded electrodes to measure resistance across epithelial and endothelial barriers. Anal. Chem. *82*, 2505–2511.

Douville, N.J., Zamankhan, P., Tung, Y.C., Li, R., Vaughan, B.L., Tai, C.F., White, J., Christensen, P.J., Grotberg, J.B., and Takayama, S. (2011). Combination of fluid and solid mechanical stresses contribute to cell death and detachment in a microfluidic alveolar model. Lab Chip *11*, 609–619.

Edington, C.D., Chen, W.L.K., Geishecker, E., Kassis, T., Soenksen, L.R., Bhushan, B.M., Freake, D., Kirschner, J., Maass, C., Tsamandouras, N., et al. (2018). Interconnected microphysiological systems for quantitative biology and pharmacology studies. Sci. Rep. *8*, 4530.

Essig, M., Terzi, F., Burtin, M., and Friedlander, G. (2001). Mechanical strains induced by tubular flow affect the phenotype of proximal tubular cells. Am. J. Physiol. Renal Physiol. *281*, F751–F762.

Even-Ram, S., and Yamada, K.M. (2005). Cell migration in 3D matrix. Curr. Opin. Cell Biol. *17*, 524–532.

Falanga, A.P., Pitingolo, G., Celentano, M., Cosentino, A., Melone, P., Vecchione, R., Guarnieri, D., and Netti, P.A. (2017). Shuttle-mediated nanoparticle transport across an in vitro brain endothelium under flow conditions. Biotechnol. Bioeng. *114*, 1087–1095.

Feinberg, A.W., Feigel, A., Shevkoplyas, S.S., Sheehy, S., Whitesides, G.M., and Parker, K.K. (2007). Muscular thin films for building actuators and powering devices. Science *317*, 1366–1370.

Ferrell, N., Desai, R.R., Fleischman, A.J., Roy, S., Humes, D.H., and Fissell, W.H. (2010). A microfluidic bioreactor with integrated transepithelial electrical resistance (TEER) measurement electrodes for evaluation of renal epithelial cells. Biotechnol. Bioeng. *107*, 707–716.

Gao, C., Sun, X., and Gillis, K.D. (2013). Fabrication of two-layer poly(dimethyl siloxane) devices for hydrodynamic cell trapping and exocytosis measurement with integrated indium tin oxide microelectrodes arrays. Biomed. Microdevices *15*, 445–451.

Ges, I.A., Brindley, R.L., Currie, K.P.M., and Baudenbacher, F.J. (2013). A microfluidic platform for chemical stimulation and real time analysis of catecholamine secretion from neuroendocrine cells. Lab Chip *13*, 4663–4673.

Ges, I.A., Currie, K., and Baudenbacher, F. (2012). Electrochemical detection of catecholamine release using planar iridium oxide electrodes in nanoliter microfluidic cell culture volumes. Biosens. Bioelectron. *34*, 30–36.

Gladkov, A., Pigareva, Y., Kutyina, D., Kolpakov, V., Bukatin, A., Mukhina, I., Kazantsev, V., and Pimashkin, A. (2017). Design of cultured neuron networks in vitro with predefined connectivity using asymmetric microfluidic channels. Sci. Rep. *7*, 15625.

Gribi, S., du Bois de Dunilac, S., Ghezzi, D., and Lacour, S.P. (2018). A microfabricated nerve-on-a-chip platform for rapid assessment of neural conduction in explanted peripheral nerve fibers. Nat. Commun. *9*, 4403.

Griep, L.M., Wolbers, F., de Wagenaar, B., ter Braak, P.M., Weksler, B.B., Romero, I.A., Couraud, P.O., Vermes, I., van der Meer, A.D., and van den Berg, A. (2013). BBB on chip: microfluidic platform to mechanically and biochemically modulate blood-brain barrier function. Biomed. Microdevices *15*, 145–150.

Grosberg, A., Alford, P.W., McCain, M.L., and Parker, K. (2011). Ensembles of engineered cardiac tissues for physiological and pharmacological study: heart on a chip. Lab Chip *11*, 4165–4173.

Hawkins, B.T., and Davis, T.P. (2005). The blood-brain barrier/neurovascular unit in health and disease. Pharmacol. Rev. *57*, 173–185.

Heileman, K., Daoud, J., and Tabrizian, M. (2013). Dielectric spectroscopy as a viable biosensing tool for cell and tissue characterization and analysis. Biosens. Bioelectron. *49*, 348–359.

Henry, O.Y.F., Villenave, R., Cronce, M.J., Leineweber, W.D., Benz, M.A., and Ingber, D.E. (2017). Organs-on-chips with integrated electrodes for trans-epithelial electrical resistance (TEER) measurements of human epithelial barrier function. Lab Chip *17*, 2264–2271.

Hickman, J. (2016). Transepithelial/endothelial Electrical Resistance (TEER) theory and applications for microfluidic body-on-a-chip devices. J. Rare Dis. Res. Treat. *1*, 46–52.

Hittinger, M., Schneider-Daum, N., and Lehr, C.M. (2017). Cell and tissue-based in vitro models for improving the development of oral inhalation drug products. Eur. J. Pharm. Biopharm. *118*, 73–78.

Hong, G., and Lieber, C.M. (2019). Novel electrode technologies for neural recordings. Nat. Rev. Neurosci. *20*, 330–345.

Huang, J.X., Blaskovich, M.A., and Cooper, M.A. (2014). Cell- and biomarker-based assays for predicting nephrotoxicity. Expert Opin. Drug Metab. Toxicol. *10*, 1621–1635.

Huebsch, N., Loskill, P., Mandegar, M.A., Marks, N.C., Sheehan, A.S., Ma, Z., Mathur, A., Nguyen, T.N., Yoo, J.C., Judge, L.M., et al. (2015). Automated video-based analysis of contractility and calcium flux in human-induced pluripotent stem cell-derived cardiomyocytes cultured over different spatial scales. Tissue Eng. Part C Methods *21*, 467–479.

Hughes, D.J., Kostrzewski, T., and Sceats, E.L. (2017). Opportunities and challenges in the wider adoption of liver and interconnected microphysiological systems. Exp. Biol. Med. *242*, 1593–1604.

Huh, D., Leslie, D.C., Matthews, B.D., Fraser, J.P., Jurek, S., Hamilton, G.A., Thorneloe, K.S., McAlexander, M.A., and Ingber, D.E. (2012). A human disease model of drug toxicity-induced pulmonary edema in a lung-on-a-chip microdevice. Sci. Transl. Med. *4*, 159ra147.

Huh, D., Matthews, B.D., Mammoto, A., Montoya-Zavala, M., Hsin, H.Y., and Ingber, D.E. (2010). Reconstituting organ-level lung functions on a chip. Science *328*, 1662–1668.

Huval, R.M., Miller, O.H., Curley, J.L., Fan, Y., Hall, B.J., and Moore, M.J. (2015). Microengineered peripheral nerve-on-a-chip for preclinical physiological testing. Lab Chip *15*, 2221–2232.

Ingber, D.E. (2016). Reverse engineering human pathophysiology with organs-on-chips. Cell *164*, 1105–1109.

Ionescu, A., Zahavi, E.E., Gradus, T., Ben-Yaakov, K., and Perlson, E. (2016). Compartmental microfluidic system for studying muscle-neuron communication and neuromuscular junction maintenance. Eur. J.Cell Biol. *95*, 69–88.

Jang, K.J., Cho, H.S., Kang, D.H., Bae, W.G., Kwon, T.H., and Suh, K.Y. (2011). Fluid-shear-stress-induced translocation of aquaporin-2 and reorganization of actin cytoskeleton in renal tubular epithelial cells. Integr. Biol. (Camb.) *3*, 134–141.

Jang, K.J., Mehr, A.P., Hamilton, G.A., McPartlin, L.A., Chung, S., Suh, K.Y., and Ingber, D.E. (2013). Human kidney proximal tubule-on-a-chip for drug transport and nephrotoxicity assessment. Integr. Biol. (Camb.) *5*, 1119–1129.

Jang, M.J., Kim, W.R., Joo, S., Ryu, J.R., Lee, E., Nam, Y., and Sun, W. (2016). Cell-type dependent effect of surface-patterned microdot arrays on neuronal growth. Front. Neurosci. *10*, 217.

Jeong, S., Kim, S., Buonocore, J., Park, J., Welsh, C.J., Li, J., and Han, A. (2018). A three-dimensional arrayed microfluidic blood-brain barrier model with integrated electrical sensor array. IEEE Trans. Biomed. Eng. *65*, 431–439.

Jiang, B. (2017). Aerobic glycolysis and high level of lactate in cancer metabolism and microenvironment. Genes Dis. *4*, 25–27.

Johnson, C., Han, Y., Hughart, N., McCarra, J., Alpini, G., and Meng, F. (2012). Interleukin-6 and its receptor, key players in hepatobiliary inflammation and cancer. Transl. Gastrointest. Cancer *1*, 58–70.

Joy, J.E., and Johnston, R.B.; Institute of Medicine Committee on Multiple Sclerosis: Current Status and Strategies for the Future (2001). In Multiple Sclerosis: Current Status and Strategies for the Future (National Academy Press).

Jungblut, M., Knoll, W., Thielemann, C., and Pottek, M. (2009). Triangular neuronal networks on microelectrode arrays: an approach to improve the properties of low-density networks for extracellular recording. Biomed. Microdevices *11*, 1269–1278.

Kanagasabapathi, T.T., Ciliberti, D., Martinoia, S., Wadman, W.J., and Decre, M.M. (2011). Dual-compartment neurofluidic system for electrophysiological measurements in physically segregated and functionally connected neuronal cell culture. Front. Neuroeng. *4*, 13.

Kanagasabapathi, T.T., Franco, M., Barone, R.A., Martinoia, S., Wadman, W.J., and Decre, M.M. (2013). Selective pharmacological manipulation of cortical-thalamic co-cultures in a dual-compartment device. J. Neurosci. Methods *214*, 1–8.

Kanagasabapathi, T.T., Massobrio, P., Barone, R.A., Tedesco, M., Martinoia, S., Wadman, W.J., and Decre, M.M. (2012). Functional connectivity and dynamics of cortical-thalamic networks co-cultured in a dual compartment device. J. Neural Eng. *9*, https://doi.org/10.1088/1741-2560/9/3/036010.

Kato, Y., Ozawa, S., Miyamoto, C., Maehata, Y., Suzuki, A., Maeda, T., and Baba, Y. (2013). Acidic extracellular microenvironment and cancer. Cancer Cell Int. *13*, 89.

Khodagholy, D., Curto, V.F., Fraser, K.J., Gurfinkel, M., Byrne, R., Diamond, D., Malliaras, G.G., Benito-Lopez, F., and Owens, R.M. (2012). Organic electrochemical transistor incorporating an ionogel as a solid state electrolyte for lactate sensing. J. Mater. Chem. *22*, https://doi.org/10.1039/c2jm15716k.

Khoshakhlagh, P., Sivakumar, A., Pace, L.A., Sazer, D.W., and Moore, M.J. (2018). Methods for fabrication and evaluation of a 3D microengineered model of myelinated peripheral nerve. J. Neural Eng. *15*, 064001.

Kim, B.N., Herbst, A.D., Kim, S.J., Minch, B.A., and Lindau, M. (2013). Parallel recording of neurotransmitters release from chromaffin cells using a 10×10 CMOS IC potentiostat array with on-chip working electrodes. Biosens. Bioelectron. *41*, 736–744.

Kim, H., Huh, D., Hamilton, G., and Ingber, D.E. (2012). Human gut-on-a-chip inhabited by microbial flora that experiences intestinal peristalsis-like motions and flow. Lab Chip *12*, 2165–2174.

Kim, H.J., Lee, J., Choi, J.-H., Bahinski, A., and Ingber, D.E. (2016a). Co-culture of living microbiome with microengineered human intestinal villi in a gut-on-a-chip microfluidic device. J. Vis. Exp. e54344, https://doi.org/10.3791/54344.

Kim, H.J., Li, H., Collins, J.J., and Ingber, D.E. (2016b). Contributions of microbiome and mechanical deformation to intestinal bacterial overgrowth and inflammation in a human gut-on-a-chip. Proc. Natl. Acad. Sci. U S A *113*, E7.

Kim, S.H., Kang, J.H., Chung, I.Y., and Chung, B.G. (2011). Mucin (MUC5AC) expression by lung epithelial cells cultured in a microfluidic gradient device. Electrophoresis *32*, 254–260.

Kirby, R., Cho, E.J., Gehrke, B., Bayer, T., Park, Y.S., Neikirk, D.P., McDevitt, J.T., and Ellington, A.D. (2004). Aptamer-based sensor arrays for the detection and quantitation of proteins. Anal. Chem. *76*, 4066–4075.

Kitsara, M., Kontziampasis, D., Agbulut, O., and Chen, Y. (2019). Heart on a chip: micro-nanofabrication and microfluidics steering the future of cardiac tissue engineering. Microelectron. Eng. *203-204*, 44–62.

Kleinfeld, D., Kahler, K.H., and Hockberger, P.E. (1988). Controlled outgrowth of dissociated neurons on patterned substrates. J. Neurosci. *8*, 4098–4120.

Koester, P., Buehler, S., Stubbe, M., Tautorat, C., Niendorf, M., Baumann, W., and Gimsa, J. (2010a). Modular glass chip system measuring the electric activity and adhesion of neuronal cells—application and drug testing with sodium valproic acid. Lab Chip *10*, 1579–1586.

Koester, P.J., Buehler, S.M., Stubbe, M., Tautorat, C., Niendorf, M., Baumann, W., and Gimsa, J. (2010b). Modular glass chip system measuring the electric activity and adhesion of neuronal cells–application and drug testing with sodium valproic acid. Lab Chip *10*, 1579–1586.

Koziolek, M., Grimm, M., Schneider, F., Jedamzik, P., Sager, M., Kuhn, J.P., Siegmund, W., and Weitschies, W. (2016). Navigating the human gastrointestinal tract for oral drug delivery: uncharted waters and new frontiers. Adv. Drug Deliv. Rev. *101*, 75–88.

Kujala, V.J., Pasqualini, F., Goss, J.A., Nawroth, J.C., and Parker, K. (2016). Laminar ventricular myocardium on a microelectrode array-based chip. J. Mater. Chem. B *4*, 3534–3543.

Lee, S., Ko, J., Park, D., Lee, S.R., Chung, M., Lee, Y., and Jeon, N.L. (2018). Microfluidic-based vascularized microphysiological systems. Lab Chip *18*, 2686–2709.

Lei, K., Tseng, H.-P., Lee, C.-Y., and Tsang, N.-M. (2016). Quantitative study of cell invasion process under extracellular stimulation of cytokine in a microfluidic device. Sci. Rep. *6*, 25557.

Levsky, J.M., and Singer, R.H. (2003). Gene expression and the myth of the average cell. Trends Cell Biol. *13*, 4–6.

Lewandowska, M.K., Bakkum, D.J., Rompani, S.B., and Hierlemann, A. (2015). Recording large extracellular spikes in microchannels along many axonal sites from individual neurons. PLoS One *10*, e0118514.

Li, M.W., and Martin, S.R. (2008). Microchip-based integration of cell immobilization, electrophoresis, post-column derivatization, and fluorescence detection for monitoring the release of dopamine from PC 12 cells. Analyst *133*, 1358–1366.

Li, M.W., Spence, D.M., and Martin, R.S. (2005). A microchip-based system for immobilizing PC 12 cells and amperometrically detecting catecholamines released after stimulation with calcium. Electroanalysis *17*, 1171–1180.

Lind, J.U., Busbee, T.A., Valentine, A.D., Pasqualini, F.S., Yuan, H., Yadid, M., Park, S.-J., Kotikian, A., Nesmith, A.P., Campbell, P.H., et al. (2016). Instrumented cardiac microphysiological devices via multimaterial three-dimensional printing. Nat. Mater. *16*, https://doi.org/10.1038/nmat4782.

Lind, J.U., Yadid, M., Perkins, I., O'Connor, B.B., Eweje, F., Chantre, C.O., Hemphill, M.A., Yuan, H., Campbell, P.H., Vlassak, J.J., et al. (2017). Cardiac microphysiological devices with flexible thin-film sensors for higher-throughput drug screening. Lab Chip *17*, 3692–3703.

Liu, X., Barizuddin, S., Shin, W., Mathai, C.J., Gangopadhyay, S., and Gillis, K.D. (2011). Microwell device for targeting single cells to electrochemical microelectrodes for high-throughput amperometric detection of quantal exocytosis. Anal. Chem. *83*, 2445–2451.

Lonardoni, D., Amin, H., Zordan, S., Boi, F., Lecomte, A., Angotzi, G.N., and Berdondini, L. (2019). Active high-density electrode arrays: technology and applications in neuronal cell cultures. Adv. Neurobiol. *22*, 253–273.

Ma, Z., Liu, Q., Liu, H., Yang, H., Yun, J.X., Eisenberg, C., Borg, T.K., Xu, M., and Gao, B.Z. (2011). Laser-patterned stem-cell bridges in a cardiac muscle model for on-chip electrical conductivity analyses. Lab Chip *12*, 566–573.

Maoz, B.M., Herland, A., Henry, O.Y.F., Leineweber, W.D., Yadid, M., Doyle, J., Mannix, R., Kujala, V.J., FitzGerald, E.A., Parker, K., et al. (2017). Organs-on-Chips with combined multi-electrode array and transepithelial electrical resistance measurement capabilities. Lab Chip *17*, 2294–2302.

Marconi, E., Nieus, T., Maccione, A., Valente, P., Simi, A., Messa, M., Dante, S., Baldelli, P., Berdondini, L., and Benfenati, F. (2012). Emergent functional properties of neuronal networks with controlled topology. PLoS One *7*, e34648.

Massry, S.G., and Glassock, R.J. (2001). Massry & glassock's textbook of nephrology, 4th edition (Lippincott Williams & Wilkins).

Megha, R., and Leslie, S.W. (2019). Anatomy, abdomen and pelvis, adrenal glands (suprarenal glands). In StatPearls (Treasure Island (FL): StatPearls Publishing), https://www.ncbi.nlm.nih.gov/books/NBK482264/.

Merrill, D.R., Bikson, M., and Jefferys, J.G. (2005). Electrical stimulation of excitable tissue: design of efficacious and safe protocols. J. Neurosci. Methods *141*, 171–198.

Michael, D.J., and Wightman, R.M. (1999). Electrochemical monitoring of biogenic amine neurotransmission in real time. J. Pharm. Biomed. Anal. *19*, 33–46.

Miller, P.G., and Shuler, M.L. (2016). Design and demonstration of a pumpless 14 compartment microphysiological system. Biotechnol. Bioeng. *113*, 2213–2227.

Monzel, A.S., Smits, L.M., Hemmer, K., Hachi, S., Moreno, E.L., van Wuellen, T., Jarazo, J., Walter, J., Bruggemann, I., Boussaad, I., et al. (2017). Derivation of human midbrain-specific organoids from neuroepithelial stem cells. Stem Cell Reports *8*, 1144–1154.

Mori, N., Morimoto, Y., and Takeuchi, S. (2017). Skin integrated with perfusable vascular channels on a chip. Biomaterials *116*, 48–56.

Morimoto, Y., Kato-Negishi, M., Onoe, H., and Takeuchi, S. (2013). Three-dimensional neuron-muscle constructs with neuromuscular junctions. Biomaterials *34*, 9413–9419.

Moutaux, E., Charlot, B., Genoux, A., Saudou, F., and Cazorla, M. (2018). An integrated microfluidic/microelectrode array for the study of activity-dependent intracellular dynamics in neuronal networks. Lab Chip *18*, 3425–3435.

Moya, A., Illa, X., Gimenez, I., Lazo-Fernandez, Y., Villa, R., Errachid, A., and Gabriel, G. (2018a). Miniaturized multiparametric flexible platform for the simultaneous monitoring of ionic: application in real urine. Sensor. Actuator. B Chem. *255*, 2861–2870.

Moya, A., Ortega-Ribera, M., Guimerà, X., Sowade, E., Zea, M., Illa, X., Ramon, E., Villa, R., Gracia-Sancho, J., and Gabriel, G. (2018b). Online oxygen monitoring using integrated inkjet-printed sensors in a liver-on-a-chip system. Lab Chip *18*, 2023–2035.

Musick, K., Khatami, D., and Wheeler, B.C. (2009). Three-dimensional micro-electrode array for recording dissociated neuronal cultures. Lab Chip *9*, 2036–2042.

Muz, B., de la Puente, P., Azab, F., and Azab, A.K. (2015). The role of hypoxia in cancer progression, angiogenesis, metastasis, and resistance to therapy. Hypoxia (Auckl.) *3*, 83–92.

Neher, E., and Sakmann, B. (1976). Single-channel currents recorded from membrane of denervated frog muscle fibres. Nature *260*, 799–802.

Nguemo, F., Šaric, T., Pfannkuche, K., Watzele, M., Reppel, M., and Hescheler, J. (2012). In vitro model for assessing arrhythmogenic properties of drugs based on high-resolution impedance measurements. Cell Physiol. Biochem. *29*, 819–832.

Nguyen, T., Yin, T.-I., Reyes, D., and Urban, G.A. (2013). Microfluidic chip with integrated electrical cell-impedance sensing for monitoring single cancer cell migration in three-dimensional matrixes. Anal. Chem. *85*, 11068–11076.

Oiwa, K., Shimba, K., Numata, T., Takeuchi, A., Kotani, K., and Jimbo, Y. (2016). A device for co-culturing autonomic neurons and cardiomyocytes using micro-fabrication techniques. Integr. Biol. (Camb.) *8*, 341–348.

Oleaga, C., Lavado, A., Riu, A., Rothemund, S., Carmona-Moran, C.A., Persaud, K., Yurko, A., Lear, J., Narasimhan, N., Long, C.J., et al. (2019). Long-term electrical and mechanical function monitoring of a human-on-a-chip system. Adv. Funct. Mater. *29*, 1805792.

Oleaga, C., Riu, A., Rothemund, S., Lavado, A., McAleer, C.W., Long, C.J., Persaud, K., Narasimhan, N., Tran, M., Roles, J., et al. (2018). Investigation of the effect of hepatic metabolism on off-target cardiotoxicity in a multi-organ human-on-a-chip system. Biomaterials *182*, 176–190.

Olson, K.L., Marc, D.T., Grude, L.A., McManus, C.J., and Kellermann, G.H. (2011). The hypothalamic-pituitary-adrenal Axis: the actions of the central nervous system and potential biomarkers. In Anti-aging Therapeutics, R. Klatz and R. Goldman, eds. (American Academy of Anti-Aging Medicine), pp. 91–100.

Ortega, M.A., Fernandez-Garibay, X., Castano, A.G., De Chiara, F., Hernandez-Albors, A., Balaguer-Trias, J., and Ramon-Azcon, J. (2019). Muscle-on-a-chip with an on-site multiplexed biosensing system for in situ monitoring of secreted IL-6 and TNF-alpha. Lab Chip *19*, 2568–2580.

Osaki, T., Sivathanu, V., and Kamm, R.D. (2018). Engineered 3D vascular and neuronal networks in a microfluidic platform. Sci. Rep. *8*, 5168.

Pan, L., Alagapan, S., Franca, E., Leondopulos, S.S., DeMarse, T.B., Brewer, G.J., and Wheeler, B.C. (2015). An in vitro method to manipulate the direction and functional strength between neural populations. Front. Neural Circuits *9*, 32.

Parrish, J., Lim, K., Zhang, B., Radisic, M., and Woodfield, T.B.F. (2019). New frontiers for biofabrication and bioreactor design in microphysiological system development. Trends Biotechnol. https://doi.org/10.1016/j.tibtech.2019.04.009.

Pedersen, B.K., and Febbraio, M.A. (2008). Muscle as an endocrine organ: focus on muscle-derived interleukin-6. Physiol. Rev. *88*, 1379–1406.

Peloso, A., Katari, R., Murphy, S.V., Zambon, J.P., DeFrancesco, A., Farney, A.C., Rogers, J., Stratta, R.J., Manzia, T.M., and Orlando, G. (2015). Prospect for kidney bioengineering: shortcomings of the status quo. Expert Opin. Biol. Ther. *15*, 547–558.

Pihel, K., Schroeder, T.J., and Wightman, R.M. (1994). Rapid and selective cyclic voltammetric measurements of epinephrine and norepinephrine as a method to measure secretion from single bovine adrenal medullary cells. Anal. Chem. *66*, 4532–4537.

Pine, J. (1980). Recording action potentials from cultured neurons with extracellular microcircuit electrodes. J. Neurosci. Methods *2*, 19–31.

Portillo-Lara, R., and Annabi, N. (2016). Microengineered cancer-on-a-chip platforms to study the metastatic microenvironment. Lab Chip *16*, 4063–4081.

Qian, F., Huang, C., Lin, Y.-D., Ivanovskaya, A.N., O'Hara, T.J., Booth, R.H., Creek, C.J., Enright, H.A., Soscia, D.A., Belle, A.M., et al. (2017). Simultaneous electrical recording of cardiac electrophysiology and contraction on chip. Lab Chip *17*, 1732–1739.

Ramadan, Q., and Ting, F.C. (2016). In vitro micro-physiological immune-competent model of the human skin. Lab Chip *16*, 1899–1908.

Riahi, R., Shaegh, S.A.M., Ghaderi, M., Zhang, Y.S., Shin, S.R., Aleman, J., Massa, S., Kim, D., Dokmeci, M.R., and Khademhosseini, A. (2016). Automated microfluidic platform of bead-based electrochemical immunosensor integrated with bioreactor for continual monitoring of cell secreted biomarkers. Sci. Rep. *6*, 24598.

Ripplinger, C.M., Noujaim, S.F., and Linz, D. (2016). The nervous heart. Prog. Biophys. Mol. Biol. *120*, 199–209.

Robelek, R., and Wegener, J. (2010). Label-free and time-resolved measurements of cell volume changes by surface plasmon resonance (SPR)

spectroscopy. Biosens. Bioelectron. *25*, 1221–1224.

Rothbauer, M., Charwat, V., Bachmann, B., Sticker, D., Novak, R., Wanzenbock, H., Mathies, R.A., and Ertl, P. (2019). Monitoring transient cell-to-cell interactions in a multi-layered and multi-functional allergy-on-a-chip system. Lab Chip *19*, 1916–1921.

Rowe, L., Almasri, M., Lee, K., Fogleman, N., Brewer, G.J., Nam, Y., Wheeler, B.C., Vukasinovic, J., Glezer, A., and Frazier, A.B. (2007). Active 3-D microscaffold system with fluid perfusion for culturing in vitro neuronal networks. Lab Chip *7*, 475–482.

Sakai, K., Shimba, K., Kotani, K., and Jimbo, Y. (2017). A co-culture microtunnel technique demonstrating a significant contribution of unmyelinated Schwann cells to the acceleration of axonal conduction in Schwann cell-regulated peripheral nerve development. Integr. Biol. (Camb.) *9*, 678–686.

Sato, T., and Clevers, H. (2013). Growing self-organizing mini-guts from a single intestinal stem cell: mechanism and applications. Science *340*, 1190–1194.

Selimovic, A., Erkal, J.L., Spence, D.M., and Martin, R.S. (2014). Microfluidic device with tunable post arrays and integrated electrodes for studying cellular release. Analyst *139*, 5686–5694.

Sellgren, K.L., Butala, E.J., Gilmour, B.P., Randell, S.H., and Grego, S. (2014). A biomimetic multicellular model of the airways using primary human cells. Lab Chip *14*, 3349–3358.

Shah, P., Fritz, J.V., Glaab, E., Desai, M.S., Greenhalgh, K., Frachet, A., Niegowska, M., Estes, M., Jäger, C., Seguin-Devaux, C., et al. (2016). A microfluidics-based in vitro model of the gastrointestinal human–microbe interface. Nat. Commun. *7*, 11535.

Sharma, A.D., McCoy, L., Jacobs, E., Willey, H., Behn, J.Q., Nguyen, H., Bolon, B., Curley, J.L., and Moore, M.J. (2019). Engineering a 3D functional human peripheral nerve in vitro using the Nerve-on-a-Chip platform. Sci. Rep. *9*, 8921.

Shin, S., Zhang, Y., Kim, D.-J., Manbohi, A., Avci, H., Silvestri, A., Aleman, J., Hu, N., Kilic, T., Keung, W., et al. (2016). Aptamer-based microfluidic electrochemical biosensor for monitoring cell-secreted trace cardiac biomarkers. Anal. Chem. https://doi.org/10.1021/acs.analchem.6b02028.

Shin, S.R., Kilic, T., Zhang, Y.S., Avci, H., Hu, N., Kim, D., Branco, C., Aleman, J., Massa, S., Silvestri, A., et al. (2017). Label-free and regenerative electrochemical microfluidic biosensors for continual monitoring of cell secretomes. Adv. Sci. *4*, 1600522.

Skardal, A., Murphy, S.V., Devarasetty, M., Mead, I., Kang, H.W., Seol, Y.J., Shrike Zhang, Y., Shin, S.R., Zhao, L., Aleman, J., et al. (2017). Multi-tissue interactions in an integrated three-tissue organ-on-a-chip platform. Sci. Rep. *7*, 8837.

Smith, A.S., Long, C.J., Pirozzi, K., and Hickman, J.J. (2013). A functional system for high-content screening of neuromuscular junctions in vitro. Technology (Singap. World Sci.) *1*, 37–48.

Son, K.J., Gheibi, P., Stybayeva, G., Rahimian, A., and Revzin, A. (2017). Detecting cell-secreted growth factors in microfluidic devices using bead-based biosensors. Microsyst. Nanoeng. *3*, 17025.

Spira, M.E., and Hai, A. (2013). Multi-electrode array technologies for neuroscience and cardiology. Nat. Nanotechnol. *8*, 83.

Sriram, G., Alberti, M., Dancik, Y., Wu, B., Wu, R., Feng, Z., Ramasamy, S., Bigliardi, P.L., Bigliardi-Qi, M., and Wang, Z. (2018). Full-thickness human skin-on-chip with enhanced epidermal morphogenesis and barrier function. Mater. Today *21*, 326–340.

Stancescu, M., Molnar, P., McAleer, C.W., McLamb, W., Long, C.J., Oleaga, C., Prot, J.-M., and Hickman, J.J. (2015). A phenotypic in vitro model for the main determinants of human whole heart function. Biomaterials *60*, 20–30.

Strakosas, X., Sessolo, M., Hama, A., Rivnay, J., Stavrinidou, E., Malliaras, G.G., and Owens, R.M. (2014). A facile biofunctionalisation route for solution processable conducting polymer devices. J. Mater. Chem. B *2*, 2537–2545.

Strakosas, X., Wei, B., Martin, D.C., and Owens, R.M. (2016). Biofunctionalization of polydioxythiophene derivatives for biomedical applications. J. Mater. Chem. B *4*, 4952–4968.

Stucki, J.D., Hobi, N., Galimov, A., Stucki, A.O., Schneider-Daum, N., Lehr, C.M., Huwer, H., Frick, M., Funke-Chambour, M., Geiser, T., et al. (2018). Medium throughput breathing human primary cell alveolus-on-chip model. Sci. Rep. *8*, 14359.

Sun, X., and Gillis, K.D. (2006). On-chip amperometric measurement of quantal catecholamine release using transparent indium tin oxide electrodes. Anal. Chem. *78*, 2521–2525.

Sung, J.H., Wang, Y.I., Narasimhan Sriram, N., Jackson, M., Long, C., Hickman, J.J., and Shuler, M.L. (2019). Recent advances in body-on-a-chip systems. Anal. Chem. *91*, 330–351.

Takeuchi, A., Nakafutami, S., Tani, H., Mori, M., Takayama, Y., Moriguchi, H., Kotani, K., Miwa, K., Lee, J.K., Noshiro, M., et al. (2011). Device for co-culture of sympathetic neurons and cardiomyocytes using microfabrication. Lab Chip *11*, 2268–2275.

Tandon, N., Cannizzaro, C., Chao, P.-H.G.H., Maidhof, R., Marsano, A., Au, H.T., Radisic, M., and Vunjak-Novakovic, G. (2009). Electrical stimulation systems for cardiac tissue engineering. Nat. Protoc. *4*, 155–173.

Tandon, N., Marsano, A., Maidhof, R., Numata, K., Montouri-Sorrentino, C., Cannizzaro, C., Voldman, J., and Vunjak-Novakovic, G. (2010). Surface-patterned electrode bioreactor for electrical stimulation. Lab Chip *10*, 692–700.

Taveggia, C., Zanazzi, G., Petrylak, A., Yano, H., Rosenbluth, J., Einheber, S., Xu, X., Esper, R.M., Loeb, J.A., Shrager, P., et al. (2005). Neuregulin-1 type III determines the ensheathment fate of axons. Neuron *47*, 681–694.

Thomas, C.A., Jr., Springer, P.A., Loeb, G.E., Berwald-Netter, Y., and Okun, L.M. (1972). A miniature microelectrode array to monitor the bioelectric activity of cultured cells. Exp. Cell Res. *74*, 61–66.

Toepke, M.W., and Beebe, D.J. (2006). PDMS absorption of small molecules and consequences in microfluidic applications. Lab Chip *6*, 1484–1486.

Trapecar, M., Communal, C., Velazquez, J., Maass, C.A., Huang, Y.-J., Schneider, K., Wright, C.W., Eng, G., Yilmaz, O., Trumper, D., et al. (2019). Gut-Liver physiomimetics reveal paradoxical modulation of IBD-related inflammation by short-chain fatty acids. bioRxiv. https://doi.org/10.1101/706812.

Uzel, S.G., Platt, R.J., Subramanian, V., Pearl, T.M., Rowlands, C.J., Chan, V., Boyer, L.A., So, P.T., and Kamm, R.D. (2016). Microfluidic device for the formation of optically excitable, three-dimensional, compartmentalized motor units. Sci. Adv. *2*, e1501429.

Vala, M., Robelek, R., Bocková, M., Wegener, J., and Homola, J. (2013). Real-time label-free monitoring of the cellular response to osmotic stress using conventional and long-range surface plasmons. Biosens. Bioelectron. *40*, 417–421.

van der Helm, M.W., Henry, O.Y.F., Bein, A., Hamkins-Indik, T., Cronce, M.J., Leineweber, W.D., Odijk, M., van der Meer, A.D., Eijkel, J.C.T., Ingber, D.E., et al. (2019). Non-invasive sensing of transepithelial barrier function and tissue differentiation in organs-on-chips using impedance spectroscopy. Lab Chip *19*, 452–463.

van der Worp, H.B., Howells, D.W., Sena, E.S., Porritt, M.J., Rewell, S., O'Collins, V., and Macleod, M.R. (2010). Can animal models of disease reliably inform human studies? PLoS Med. *7*, e1000245.

van der Helm, M.W., van der Meer, A.D., Eijkel, J.C., van den Berg, A., and Segerink, L.I. (2016). Microfluidic organ-on-chip technology for blood-brain barrier research. Tissue Barriers *4*, e1142493.

Van Gele, M., Geusens, B., Brochez, L., Speeckaert, R., and Lambert, J. (2011). Three-dimensional skin models as tools for transdermal drug delivery: challenges and limitations. Expert Opin. Drug Deliv. *8*, 705–720.

van Meer, B.J., de Vries, H., Firth, K.S.A., van Weerd, J., Tertoolen, L.G.J., Karperien, H.B.J., Jonkheijm, P., Denning, C., IJzerman, A.P., and Mummery, C.L. (2017). Small molecule absorption by PDMS in the context of drug response bioassays. Biochem. Biophys. Res. Commun. *482*, 323–328.

Vogel, P.A., Halpin, S.T., Martin, R.S., and Spence, D.M. (2011). Microfluidic transendothelial electrical resistance measurement device that enables blood flow and postgrowth experiments. Anal. Chem. *83*, 4296–4301.

Walter, F.R., Valkai, S., Kincses, A., Petnehazi, A., Czeller, T., Veszelka, S., Ormos, P., Deli, M.A., and Der, A. (2016). A versatile lab-on-a-chip tool for modeling biological barriers. Sensor. Actuator. B Chem. *222*, 1209–1219.

Wang, Y.I., Abaci, H.E., and Shuler, M.L. (2017). Microfluidic blood-brain barrier model provides in vivo-like barrier properties for drug permeability screening. Biotechnol. Bioeng. *114*, 184–194.

Weltin, A., Slotwinski, K., Kieninger, J., Moser, I., Jobst, G., Wego, M., Ehret, R., and Urban, G.A. (2013). Cell culture monitoring for drug screening and cancer research: a transparent, microfluidic, multi-sensor microsystem. Lab Chip *14*, 138–146.

Wheeler, B.C., and Brewer, G.J. (2010). Designing Neural Networks in Culture: experiments are described for controlled growth, of nerve cells taken from rats, in predesigned geometrical patterns on laboratory culture dishes. Proc. IEEE Inst. Electr.Electron. Eng. *98*, 398–406.

Wilmer, M.J., Ng, C., Lanz, H.L., Vulto, P., Suter-Dick, L., and Masereeuw, R. (2016). Kidney-on-a-Chip technology for drug-induced nephrotoxicity screening. Trends Biotechnol. *34*, 156–170.

Winer, J.B. (2014). An update in guillain-barre syndrome. Autoimmune Dis. *2014*, 793024.

Wolf, K., Zarkua, G., Chan, S.A., Sridhar, A., and Smith, C. (2016). Spatial and activity-dependent catecholamine release in rat adrenal medulla under native neuronal stimulation. Physiol. Rep. *4*, https://doi.org/10.14814/phy2.12898.

Xu, H., Li, Z., Yu, Y., Sizdahkhani, S., Ho, W.S., Yin, F., Wang, L., Zhu, G., Zhang, M., Jiang, L., et al. (2016). A dynamic in vivo-like organotypic blood-brain barrier model to probe metastatic brain tumors. Sci. Rep. *6*, 36670.

Yang, M., and Zhang, X. (2007). Electrical assisted patterning of cardiac myocytes with controlled macroscopic anisotropy using a microfluidic dielectrophoresis chip. Sensor. Actuator. Phys. *135*, 73–79.

Yin, S.H., Zhang, X.Q., Zhan, C., Wu, J.T., Xu, J.C., and Cheung, J. (2005). Measuring single cardiac myocyte contractile force via moving a magnetic bead. Biophys. J. *88*, 1489–1495.

Zahavi, E.E., Ionescu, A., Gluska, S., Gradus, T., Ben-Yaakov, K., and Perlson, E. (2015). A compartmentalized microfluidic neuromuscular co-culture system reveals spatial aspects of GDNF functions. J.Cell Sci. *128*, 1241–1252.

Zeck, G., and Fromherz, P. (2001). Noninvasive neuroelectronic interfacing with synaptically connected snail neurons immobilized on a semiconductor chip. Proc. Natl. Acad. Sci. U S A *98*, 10457–10462.

Zhang, B., and Radisic, M. (2017). Organ-on-a-chip devices advance to market. Lab Chip *17*, 2395–2420.

Zhang, X., Wang, T., Wang, P., and Hu, N. (2016). High-throughput assessment of drug cardiac safety using a high-speed impedance detection technology-based heart-on-a-chip. Micromachines (Basel) *7*, 122.

Zhang, Y.S., Aleman, J., Shin, S.R., Kilic, T., Kim, D., Mousavi Shaegh, S.A., Massa, S., Riahi, R., Chae, S., Hu, N., et al. (2017). Multisensor-integrated organs-on-chips platform for automated and continual in situ monitoring of organoid behaviors. Proc. Natl. Acad. Sci. U S A *114*, E2293–E2302.

Zhao, Y., and Zhang, X. (2006). Cellular mechanics study in cardiac myocytes using PDMS pillars array. Sensor. Actuator. Phys. *125*, 398–404.

Zhou, Q., Patel, D., Kwa, T., Haque, A., Matharu, Z., Stybayeva, G., Gao, Y., Diehl, A.M., and Revzin, A. (2015). Liver injury-on-a-chip: microfluidic co-cultures with integrated biosensors for monitoring liver cell signaling during injury. Lab A Chip *15*, 4467–4478.